Universidade Federal do Rio Grande do Sul

Instituto de Física

Four-Well Quantum Tunneling Models for Interferometry

Erik Cardenas Giordani

Trabalho de Conclusão de Curso apresentado para a obtenção do grau de Bacharel em Física
Orientadora: Prof. Dra. Angela Foerster
Coorientador: Prof. Dr. Leandro Hayato Ymai

Porto Alegre - RS

2021

Abstract

In this work we investigate integrable models for systems with four potential wells containing Bose-Einstein condensates linked by quantum tunneling, in the open and closed configurations, presenting their hamiltonians, energy bands, regimes and dynamics with dependencies on different parameters. Focusing on resonant regimes, we analyse fidelities and entanglement and highlight relevant properties and applications in interferometry, presenting two different interferometer models, their sensitivities and other properties.

Resumo

Neste trabalho investigamos modelos integráveis para sistemas com quatro poços de potencial contendo condensados de Bose-Einstein ligados por tunelamento quântico, nas configurações aberta e fechada, apresentando seus hamiltonianos, bandas de energia, regimes e dinâmicas com dependências em diferentes parâmetros. Focando em regime ressonantes, analisamos fidelidades e emaranhamento e destacamos propriedades relevantes e aplicações em interferometria, apresentando dois modelos de interferômetros diferentes, suas sensitividades e outras propriedades.

Contents

1 Introduction **5**

2 Four-Well Model - Closed Arrangement **7**
2.1 Hamiltonian and Effective Hamiltonian 7
2.2 Regimes and Energy Bands 8
2.3 Fock States and The Uber-NOON 10
2.4 Fidelity and Entanglement Dynamics 11
2.5 Interferometer 14

3 Four-Well Model - Open Arrangement **17**
3.1 Hamiltonian and Effective Hamiltonian 17
3.2 Regimes and Energy Bands 17
3.3 Interferometer 19
3.3.1 Phase Control Protocol 20
3.3.2 Experimental Setup 22

4 Conclusion **24**

A Matrix Representation of Hamiltonians **25**

B Effective Hamiltonian Calculations **26**

C Calculations for the Interferometers **30**

D Other Dynamics **39**

1 Introduction

The Bose-Einstein condensate, proposed by S. N. Bose [1] and Albert Einstein [2] in 1924, is the state in which all bosons in a sample occupy the ground state, creating a degenerate gas. This behaviour is based on the wave nature of particles: In an ultra-cold condensate (temperature near absolute zero) the de Broglie wavelength is similar to the mean distance between atoms. The experimental realization was achieved, after seventy years of technological advancements , by Eric Cornell and Carl Wieman [3] and Wolfgang Ketterle [4], paving way for further research of models and applications, using vaporization and lasers for the cooling process [5]. Among such models are the exactly solvable systems [6–8] and integrable models with four potential wells containing Bose-Einstein condensates linked by quantum tunneling.

The study of exactly solvable models in Quantum Mechanics was kick-started by the analytical solution for the non-relativistic Hydrogen atom proposed by Schrodinger [9]; however, specially in cases containing many particles, analytically exact treatments remained rarely viable. In 1931, while studying the Heisenberg model [10], Bethe proposed an ansatz to obtain eigenvectors and eigenvalues from exactly solvable hamiltonians, such as the ones presented in this work. This field later received contributions from Yang [11], Baxter [12], Lieb [13] and others. Nowadays there is a considerable list of integrable systems which are relevant in areas such as statistical mechanics [14], field theory [15, 16], condensed matter physics [17, 18] and atomic and molecular physics [19, 20].

Quantum systems are usually too complex to be studied purely through analytical means (even in integrable cases), demanding the utilization of numerical and computational methods to tackle coupled and non-linear equations. The eigenvectors and eigenvalues (energies) can also be obtained through exact diagonalization of the hamiltonians, and quantum dynamics simulations can be performed with a diverse range of coupling parameters in order to identify different tunneling regimes and study the temporal behaviour of these systems, tracking variables such as number of particles, fidelity and entanglement.

This work focuses on the study of integrable tunneling models for systems of Bose-Einstein condensates with four potential wells in their closed and open configurations, distinguishable by the number of bosons in each class and their geometry (see figures below and more details in the following sections), making these potentially great candidates to describe physical properties relevant for quantum technology and realization of atomtronic devices [21, 22] (based on circuits with atomic currents, analogous to existing electronic or optical systems) for quantum metrology.

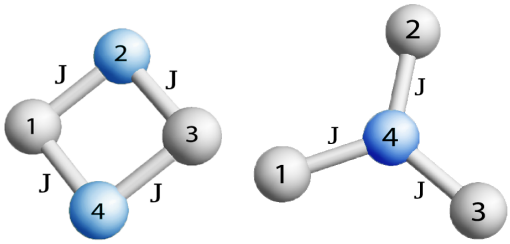

Figure 1: Geometry of the models. Different classes represented by different colours. J is the tunneling parameter. Left: Four-Well, closed arrangement. Right: Four-Well, open arrangement.

Integrability in such systems results from derivation through an extension of the Quantum Inverse Scattering Method [23–25] , introducing two conserved charges associated to resonant dynamics [26, 27], which, along with the number of particles and total energy, add up to four conserved operators, equal to the number of degrees of freedom, satisfying Liouville's requirements for integrability [28] and playing a fundamental role in the control of these systems. These conserved quantities are used to model effective hamiltonians in resonant regimes, which are very useful for the obtainment of analytical results in quantum dynamics.

There are conclusive results for self-trapping phenomena with two wells [29–34] and the usage of three-well systems [35–37] as ultra-cold transistors [38], for example. A class of models for physical realization of Heisenberg-limited [39] atomtronic phase-interferometry using dipolar atoms in four-well systems was identified in 2010 [40] and recent research focusing on both the open [41–43] and closed [44] arrangements, such as the proposal of an interferometer based on NOON states [45], aim to advance the field of quantum information and integrability-enhanced atomtronic technologies, a relatively new subfield of ultracold atomic physics. Here we revisit some of these studies, specially the closed integrable four-well system, and also make further progress in the analysis of the integrable open four-well model.

The sections in this work are organized as follows: In chapter two, the four-well model in closed arrangement is presented, along with its hamiltonian and effective hamiltonian, followed by subsections defining its different regimes, energy bands, Fock state distributions, fidelity, entanglement and finishing with a subsection dedicated to the NOON state interferometer model. Chapter three focuses on the four-well model in open arrangement, once again presenting its hamiltonians, regimes and energy bands, leading into original contributions and the proposal of an open arrangement interferometer. The appendices include the matrix representation of the hamiltonians, in depth calculations for the effective hamiltonians and interferometers, and other interesting dynamics studied.

2 Four-Well Model - Closed Arrangement

In this chapter we will review the four-well Bose-Einstein condensate model in a closed arrangement, named after its characteristic geometry containing four potential wells linked by tunneling, illustrated in the figure below.

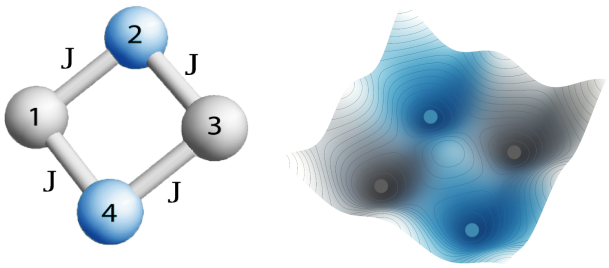

Figure 2: Left: Geometry of the four well system in closed arrangement, where J is the tunneling parameter. Right: 3D representation of the potential wells. Subspaces separated by colour.

In this configuration there are two subspaces, class A (grey) is composed of wells 1 and 3, while class B (blue) is composed of wells 2 and 4. As seen in figure 2, wells in the same class are not connected by the tunneling parameter J, thus the transition of dipolar bosons between them are limited to second order processes.

2.1 Hamiltonian and Effective Hamiltonian

The hamiltonian for the isotropic integrable model with no external potential can be modeled by:

$$H_{2,2} = -U(N_1 - N_2 + N_3 - N_4)^2 + \frac{J}{2}[(a_1^\dagger + a_3^\dagger)(a_2 + a_4) + (a_2^\dagger + a_4^\dagger)(a_1 + a_3)] \tag{2.1.1}$$

where $\{a_j, a_j^\dagger : j = 1, 2, 3, 4\}$ are canonical boson annihilation and creation operators, U characterizes the interactions between bosons, N_j is the number of particles in a well and J the tunneling strength. Distinct regimes, with different applications, may be obtained depending on the values chosen for these parameters.

This work focuses on cases where the bosons tend to be restricted to their respective classes ($M = N_1 + N_3$ and $P = N_2 + N_4$ constant) and the energy levels separate into bands (see figure 4), characterizing the resonant tunneling regime. Thus, considering second-order tunneling processes (see appendix B), the following effective hamiltonian is obtained utilizing time-dependent perturbation theory for an initial Fock state $|M-l, P-k, l, k\rangle$ and the resonance condition $J \ll U|M-P|$,

where $M + P = N$:

$$H_{\text{eff}} = (N+1)\Omega(Q_1 + Q_2) - 2\Omega Q_1 Q_2 \tag{2.1.2}$$
$$\Omega = J^2/(4U((M-P)^2 - 1))$$
$$Q_1 = \frac{1}{2}(N_1 + N_3 - a_1^\dagger a_3 - a_3^\dagger a_1)$$
$$Q_2 = \frac{1}{2}(N_2 + N_4 - a_2^\dagger a_4 - a_4^\dagger a_2)$$

Above Q_i are the remaining conserved operators (called conserved charges) needed to match the number of degrees of freedom and guarantee integrability according to the Liouville–Arnold theorem.

In order to facilitate the obtainment the eigenvectors and eigenvalues of the hamiltonians, we use the matrix representation described in appendix A.

2.2 Regimes and Energy Bands

Depending on the parameters chosen for the hamiltonian, different dynamic regimes can be identified. The image below illustrates different dynamics for the normalized expected number of particles in each well, varying U. The parameters $J/\hbar = 73.219$ Hz, $U/\hbar = 76.519$ Hz and $N = 15$ are based on existing research [44] to obtain faster resonant dynamics in a closed-arrangement system with the integrability condition.

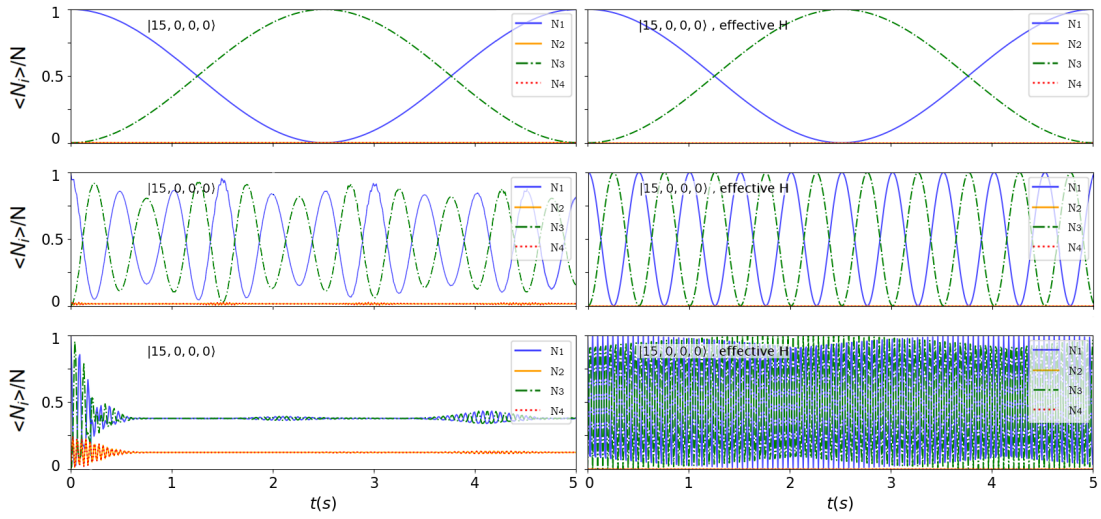

Figure 3: Dynamics in different regimes for the initial state $|15, 0, 0, 0\rangle$, using $H_{2,2}$ (left) and H_{eff} (right). $J/\hbar = 73.219$ Hz and the parameter U is varied. First row: $U/\hbar = 76.519$ Hz. Second row: $U/\hbar = 7.6519$ Hz. Third row: $U/\hbar = 0.76519$ Hz.

We can examine the image above by analysing the parameter $\chi = UN/J$. In the first row we visualize the Josephson regime, characterized by $N^2 \gg \chi \gg 1$, where the interaction parameter U dominates the dynamics, resulting in resonant tunneling. In this case, wells 2 and 4 (class B) never receive bosons from class A

and it is clear from the picture that the effective hamiltonian yields the expected results, since it was modeled for resonant tunneling regime with $J \ll U|M-P|$.

Increasing the value of χ slows down the period of the harmonic oscillation observed, eventually resulting in the Fock Regime, with $\chi \gg N^2$. This regime would appear stationary in the time-frame used for the graphs.

In the second row χ was decreased, allowing the tunneling parameter J to visibly affect the amplitude and frequency of the dynamics and we notice a significant difference between the results using $H_{2,2}$ and H_{eff}. This region is near the limit of $\chi = 1$ shown in figure 4.

In the third row, the graph on the left contains a short transient section, in which bosons are transferred to wells 2 and 4, followed by a stable state. The effective hamiltonian fails to reproduce these results (wells 2 and 4 never receive bosons). Lowering χ even further will extend the transient, this dominance of the tunneling parameter characterizes the Rabi Regime ($1 \gg \chi$).

Another way to visualize these regimes is with the energy band plot, where each line corresponds to a state $|M-l, P-k, l, k\rangle$ ($l = 0, ..., M$; $k = 0, ..., P$; $P = 0, ..., N$) for a given $N = M + P$:

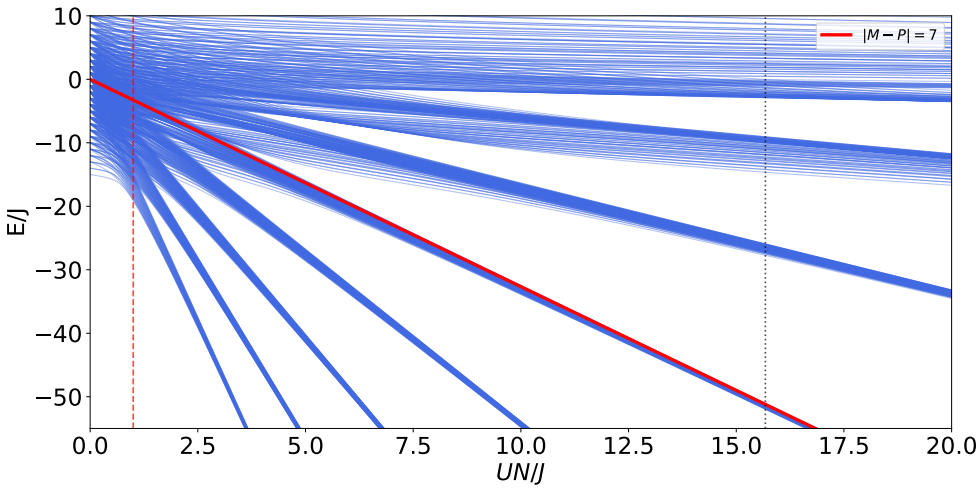

Figure 4: Dimensionless energy eigenvalues E/J as a function of dimensionless coupling $UN/J = \chi$, with $N = 15$ and $J/\hbar = 73.219$ Hz, using hamiltonian 2.1.1. Vertical lines at $\chi = 1$ (red), where the formation of bands starts, and $\chi = 15.676$, where $U/\hbar = 76.519$ Hz. The diagonal red line follows the equation: $E/J = -\chi(M-P)^2/N$, with $|M-P| = 7$.

The region before the vertical line at $\chi = 1$ has no defined bands and constitutes the Rabi regime. To the right of this line the energy levels tend to degenerate into bands as the dimensionless coupling parameter UN/J increases, the number of bands is $(N+2)/2$ if N is even and $(N+1)/2$ if N is odd. In this region we can find the Josephson regime, gradually transitioning into the Fock regime as UN/J increases.

Since the condition for the resonant tunneling regime ($J \ll U|M-P|$) depends on M and P, for each value there is a different limit in U for the formation of a band with resonant regime. Some of the blue energy levels are very close to the idealized red line at $UN/J = 15.676$, indicating harmonic oscillation in the dynamics for for $|M-P| = 7$, while other regions still contain different spacing between the lines, indicating disturbed dynamics.

2.3 Fock States and The Uber-NOON

At any point in time, the expected number of particles in each well, $\langle N_i \rangle$, results from a probability distribution over all possible Fock states with the same total number of bosons, N. Often each individual Fock state has a small probability, but in special cases such as the Uber-NOON only a few states can occur, allowing for high precision phase measurements (as shown in subsection 2.5), thus, Fock state probability histograms (see figure 5) are a useful tool to identify systems. This section focuses on resonant dynamics with initial state $|11,4,0,0\rangle$ and the parameters $U/\hbar = 76.519$ Hz and $J/\hbar = 73.219$ Hz in order to analyse Uber-NOON formation. The Uber-NOON state is characterized by an equal probability of obtaining $|M,0,0,P\rangle$, $|M,P,0,0\rangle$, $|0,0,M,P\rangle$ and $|0,P,M,0\rangle$ (and probability zero for other Fock states). The Uber-NOON has the general form

$$|\mathrm{U-NOON}\rangle = \frac{1}{2}\left(|M,P,0,0\rangle + e^{i\varphi_1}|M,0,0,P\rangle + e^{i\varphi_2}|0,P,M,0\rangle + e^{i\varphi_3}|0,0,M,P\rangle\right) \tag{2.3.1}$$

for a set of phases $\{\varphi_1, \varphi_2, \varphi_3\}$.

By plotting the Fock state probability histogram, as well as the expected number of particles in each well separately, we can detect the formation of an Uber-NOON state at $t = t_m = \hbar\pi/2\Omega \approx 4.3047s$.

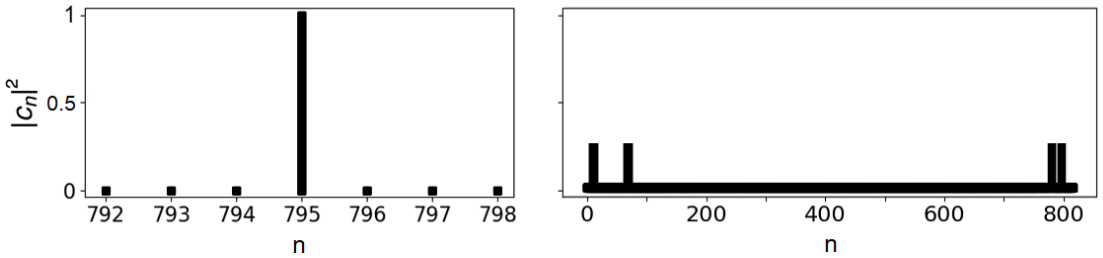

Figure 5: Probabilities $|c_n|^2$ of Fock states $|n\rangle$ for $|\Psi(t)\rangle = e^{-itH_{2,2}/\hbar}|\Psi_0\rangle = \sum_{n=0}^{D-1} c_n(t)|n\rangle$, labeled by the arbitrary single index n, where $D = (N+3)!/(3!N!)$ is the dimension of the Hilbert space. Left: The initial state is $|\Psi_0\rangle = |11,4,0,0\rangle$ ($n = 795$). Right: At $t = t_m$ there is a combination of $|0,0,11,4\rangle$ ($n = 11$), $|0,4,11,0\rangle$ ($n = 69$), $|11,0,0,4\rangle$ ($n = 781$) and $|11,4,0,0\rangle$ ($n = 795$).

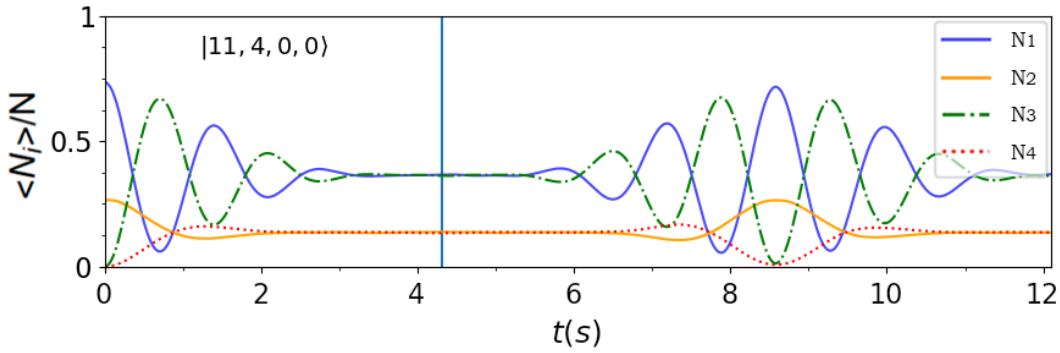

Figure 6: Dynamics for the initial state $|11,4,0,0\rangle$. $U/\hbar = 76.519$ Hz and $J/\hbar = 73.219$ Hz. Vertical line at $t = t_m$, when the system can be described by a combination of $|0,0,11,4\rangle$, $|0,4,11,0\rangle$, $|11,0,0,4\rangle$ and $|11,4,0,0\rangle$.

These results are valid for odd N, for dynamics with even N see appendix D.

2.4 Fidelity and Entanglement Dynamics

The fidelity is a parameter that allows us to analyze the amplitude and frequency of a resonant tunneling system, comparing the temporal evolution of the system to its initial state:

$$F = |\langle \Psi_0 | \Psi(t) \rangle|^2 \tag{2.4.1}$$

with $|\Psi(t)\rangle = e^{-itH_{2,2}/\hbar}|\Psi_0\rangle = \sum_{n=0}^{D-1} c_n(t)|n\rangle$[1] and F ranging from zero (completely different states) to one (identical configuration).

Figure 7 illustrates fidelity dynamics for the three examples of regimes shown previously (figure 3), with $|\Psi_0\rangle = |15,0,0,0\rangle$. It can be seen that in the resonant Josephson regime the initial state can be recovered to a high degree of accuracy ($F \approx 1$ using $H_{2,2}$ (black) and $F = 1$ using H_{eff} (red)), with almost the entire boson population periodically tunneling back.

[1]The mapping from Fock state $|i,j,k,N-i-j-k\rangle$ to state $|n = f(i,j,k)\rangle$ can be performed using the function $f : \mathbb{N}^3 \to \mathbb{N}$, defined as $f(i,j,k) = k + \frac{j}{2}[2(N-i)+3-j] + \frac{i}{2}[4+(N+2)(N-i)+2N] + \frac{i}{6}(i^2-1)$.

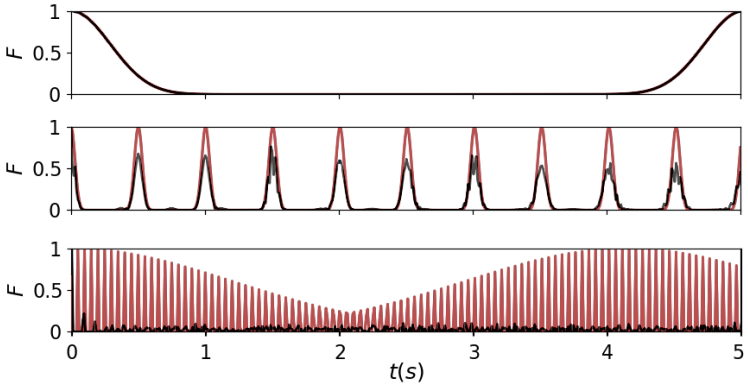

Figure 7: Fidelity dynamics in different regimes for the initial state $|15, 0, 0, 0\rangle$. The black and red curves are obtained using $H_{2,2}$ and H_{eff} respectively. $J/\hbar =$ 73.219 Hz. Top: $U/\hbar = 76.519$ Hz (Josephson, resonant). Middle: $U/\hbar = 7.6519$ Hz (transition). Bottom: $U/\hbar = 0.76519$ Hz (Rabi).

The fidelity graph can also be plotted in order to detect the formation of an Uber-NOON state by replacing $|\Psi_0\rangle$ in equation 2.4.1 with:

$$|\Psi_{NOON}\rangle = \frac{1}{2}(\beta|11, 4, 0, 0\rangle + |11, 0, 0, 4\rangle + |0, 4, 11, 0\rangle - \beta|0, 0, 11, 4\rangle) \qquad (2.4.2)$$

(Obtained by following the second protocol in [44]). With $\beta = (-1)^{(N+1)/2} = 1$ since the chosen N is odd (for the case with even N see appendix D).

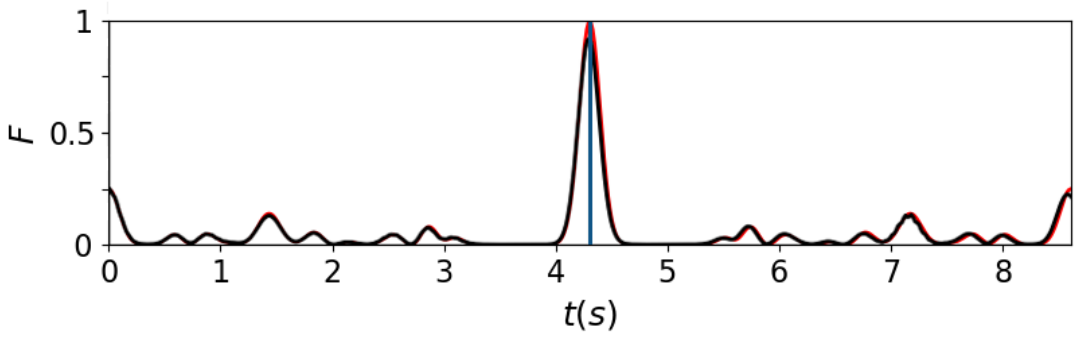

Figure 8: Fidelity vs. time for the Uber-NOON state. $U/\hbar = 76.519$ Hz and $J/\hbar = 73.219$ Hz. The black and red curves are obtained using $H_{2,2}$ and H_{eff} respectively. Vertical line at $t = t_m$.

We can see that the fidelity starts at ≈ 0.25, due to the initial state being $|11, 4, 0, 0\rangle$, and eventually approaches this value again due to the periodic nature of the system. At $t = t_m$, when the Uber-NOON state is achieved, the fidelity reaches ≈ 1. Other peaks occur throughout the graph, but they do not reach Uber-NOON state, implying that in these cases there are more than four Fock states contributing to each $\langle N_i\rangle$.

Another way to analyse systems is by studying their entanglement dynamics. First, we define the density matrix:

$$\rho(t) = |\Psi(t)\rangle\langle\Psi(t)| \tag{2.4.3}$$

and express the reduced density matrices in a compact notation:

$$\rho_j(t) = \mathrm{tr}_{pqr}\rho(t) = \sum_{i=0}^{N} P(N_j = i)|i\rangle\langle i|, \tag{2.4.4}$$

where tr_{pqr} denotes the partial trace over the state space for wells p, q and r, and $P(N_j = i)$ is the probability of measuring i bosons in well j ($j \neq p \neq q \neq r$).

Then, the von Neumann entropy, which quantifies the entanglement between the subsystems within the class of well j, is defined as

$$S_j(\rho(t)) = -\mathrm{tr}(\rho_j(t)\log\rho_j(t)) \tag{2.4.5}$$

We also define the effective von Neumann entropy $S_j(\tilde{\rho}(t))$, which is calculated through $|\tilde{\Psi}(t)\rangle = \exp(-itH_{\text{eff}}/\hbar)|\Psi_0\rangle$.

The entanglement plot below indicates that the aforementioned smaller peaks in the NOON-fidelity graph are a result of combinations of many Fock states when compared to the Uber-NOON formation at $t = t_m$, where S_2 drops significantly.

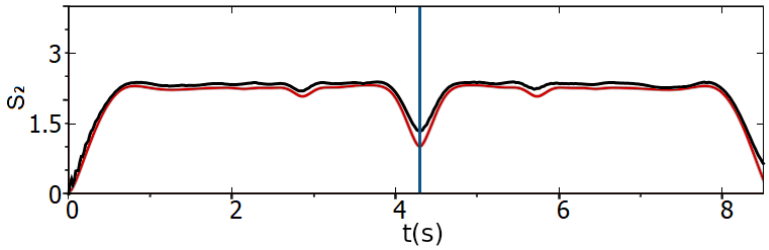

Figure 9: Entanglement dynamics for the initial state $|11, 4, 0, 0\rangle$, $U/\hbar = 76.519$ Hz and $J/\hbar = 73.219$ Hz. The black and red curves are obtained using $H_{2,2}$ and H_{eff} respectively. Vertical line at $t = t_m$.

The image below illustrates entanglement dynamics for the three examples of regimes shown previously. Once again, $H_{2,2}$ and H_{eff} yield the same results in the resonant regime, reaching zero at $t = 2.5s$ (half the period), where a single Fock state appears ($|0, 0, 15, 0\rangle$ see figure 3), and at $t = 5s$, when the initial state is recovered.

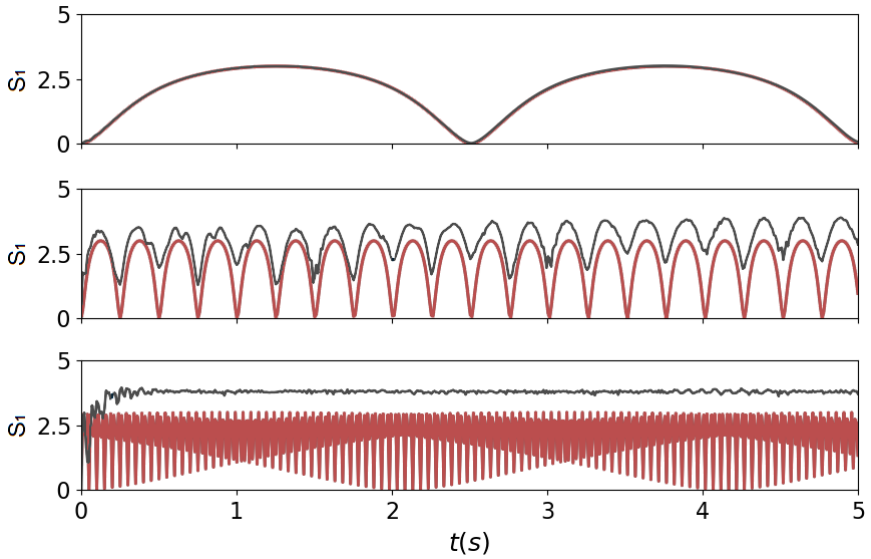

Figure 10: Entanglement dynamics in different regimes for the initial state $|15, 0, 0, 0\rangle$. The black and red curves are obtained using $H_{2,2}$ and H_{eff} respectively. $J/\hbar = 73.219$ Hz. Top: $U/\hbar = 76.519$ Hz (Josephson, resonant). Middle: $U/\hbar = 7.6519$ Hz (transition). Bottom: $U/\hbar = 0.76519$ Hz (Rabi).

2.5 Interferometer

The formation of NOON states in four-well systems in closed arrangement opens the possibility for integrability-enhanced atomtronic interferometry, with protocols based on resonant dynamics with odd N. The figure below shows a schematic representation of an interferometer:

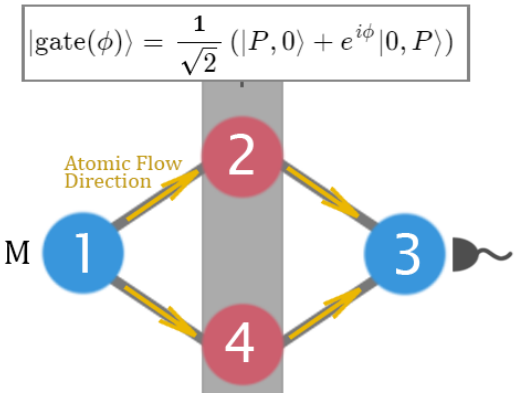

Figure 11: Schematic representation of the protocol. M atoms initially in well 1 interact with the gate (NOON state) in subspace B. After a period t_m the number of particles in well 3 follows an interference pattern.

We start with the entangled gate state in subspace B (which can be obtained with a short break of integrability, following the protocols in [44]), while subspace A has M particles in well 1 and zero in well 3.

Using $J/\hbar = 73.219$ Hz, $U/\hbar = 76.519$ Hz , $M = 11, P = 4$ and $N = M + P = 15$, this state is described by:

$$|\Psi_0\rangle = (|11, 4, 0, 0\rangle + e^{i\phi}|11, 0, 0, 4\rangle)/\sqrt{2} \tag{2.5.1}$$

We then let the system evolve until $t_m = \hbar\pi/2\Omega \approx 4.3047s$ and measure the number of bosons in well 3, obtaining the interference pattern calculated in appendix C:

$$\begin{aligned} \Delta N_3 &= \frac{1}{2}(N - P)|\sin\phi| \\ \langle N_3\rangle &= M\cos^2\left(\phi/2 - \left[1 + (-1)^{(N+1)/2}\right]\frac{\pi}{4}\right) \end{aligned} \tag{2.5.2}$$

Plugging our usual values, this results in $\langle N_3\rangle/M = \cos^2(\frac{\phi-\pi}{2})$, with a maximum at $\phi = \pi$, seen in the figure below:

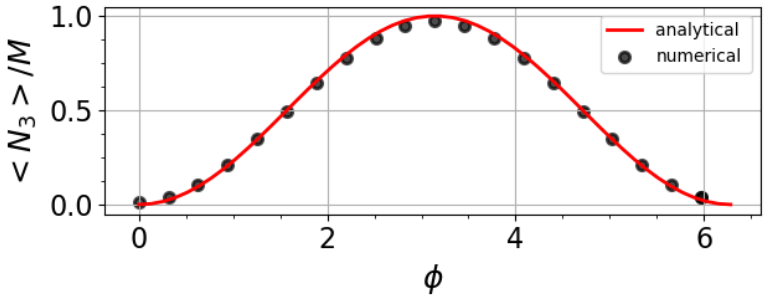

Figure 12: $\langle N_3\rangle/M$ distribution at $t = t_m$, depending on the phase ϕ. Analytical results obtained using equation 2.6.1, numerical results obtained using equation 2.1.1.

We can also plot $\langle N_3\rangle/M$ versus time for different values of ϕ to visualize its influence in the expected number of bosons at $t = t_m$.

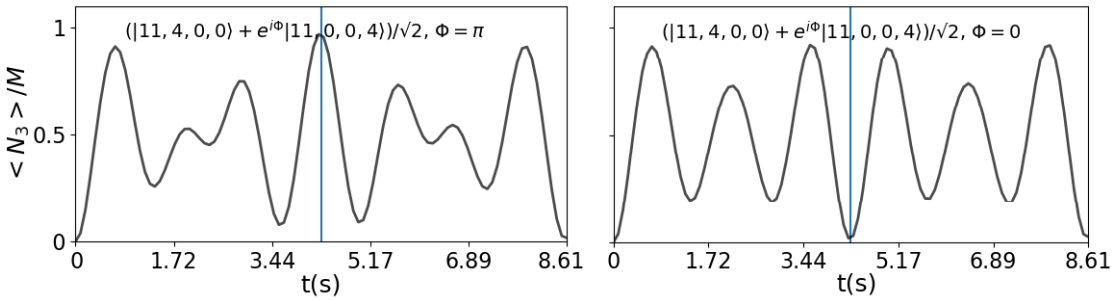

Figure 13: Expectation value dynamics using $U/\hbar = 76.519$ Hz and $J/\hbar = 73.219$ Hz. Initial states: $(|11, 4, 0, 0\rangle + e^{i\phi}|11, 0, 0, 4\rangle)/\sqrt{2}$ with $\phi = 0$ on the right and $\phi = \pi$ on the left. Vertical lines at $t = t_m$.

This model is capable of achieving Heisenberg-limited interferometry, more precise than classical protocols and equivalent to choosing the equality sign in the

Heisenberg uncertainty relation [39], with a sensitivity of

$$\Delta\varphi = \frac{\Delta N_3}{|d\langle N_3\rangle/d\varphi|} = \frac{1}{P} \tag{2.5.3}$$

For $\phi = P\varphi$ in equation (2.5.1) (see appendix C).

This phase is encoded via the transformation $a_4^\dagger \to e^{i\varphi}a_4^\dagger$ to achieve phase-super-resolution, since ϕ and its oscillations are multiplied by P, requiring a smaller variation of φ to complete a cycle.

A possible experimental setup for this model in an optical lattice formed by sets of counter-propagating beams is proposed in [44], where a complete explanation can be found. In this setup the four potential wells are isolated from the rest of the lattice by a vertical beam and the phase is encoded using an off-center laser beam to shift the potential to well 4, breaking integrability. We notice here that the breaking of integrability has also been discussed in other physical scenarios (see, for instance [46–48]). A similar model for open-arrangement interferometry is proposed at the end of the following section.

3 Four-Well Model - Open Arrangement

In this chapter we will present the Four-Well model in open arrangement, named after its characteristic geometry containing four potential wells linked by tunneling, shown in the figure below.

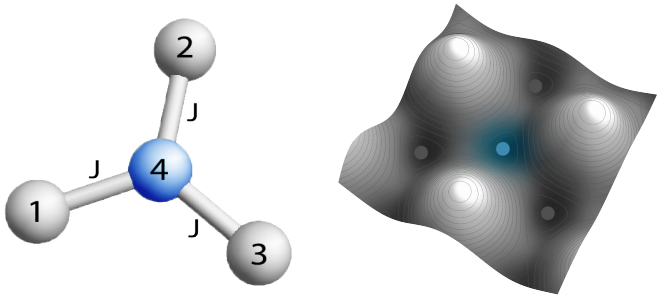

Figure 14: Left: Geometry of the four well system in open arrangement, J is the tunneling parameter. Right: 3D representation of the potential wells. The subspaces are separated by colour.

In this configuration there are two subspaces, class A (grey) is composed of wells 1, 2 and 3, while class B (blue) is composed only of well 4. Transitions between wells in the same class are limited to second order processes.

3.1 Hamiltonian and Effective Hamiltonian

The hamiltonian for the isotropic integrable model with no external potential can be modeled by:

$$H_{3,1} = -U(N_1 + N_2 + N_3 - N_4)^2$$
$$-\frac{J}{\sqrt{3}}[(a_1^\dagger + a_2^\dagger + a_3^\dagger)a_4 + a_4^\dagger(a_1 + a_2 + a_3))] \tag{3.1.1}$$

Once again we focus on the resonant regime, where the number of particles in each subspace remains constant. In this regime, the following effective hamiltonian can be derived (see appendix B):

$$H_{\text{eff}} = J_{\text{eff}}[(a_1^\dagger a_2 + a_2^\dagger a_1) + (a_1^\dagger a_3 + a_3^\dagger a_1) + (a_2^\dagger a_3 + a_3^\dagger a_2)] \tag{3.1.2}$$

$$J_{\text{eff}} = \frac{J^2(N+1)}{12U(N-2P-1)(N-2P+1)} \tag{3.1.3}$$

Since subspace B contains only one well, the number of bosons in this well remains constant in resonant regime and therefore a_4 and $a_4^\dagger$ do not appear in equation 3.1.2.

3.2 Regimes and Energy Bands

Similarly to the closed arrangement shown previously, the four-well model in open arrangement can be divided into different regimes depending on the parameter $\chi = UN/J$ (see chapter 2.2).

In the figure below we can see a clear difference in the resonant dynamics of the number of particles in each well when compared to the closed arrangement (see Figure 3) using the same values for U, J and N. In this case, the particles initially in well 1 tunnel to both well 2 and 3 and the resonant oscillations occurs around $(N_1 + N_2 + N_3)/3$ (or 1/3 in this specific, and normalized, case with $N_4 = 0$).

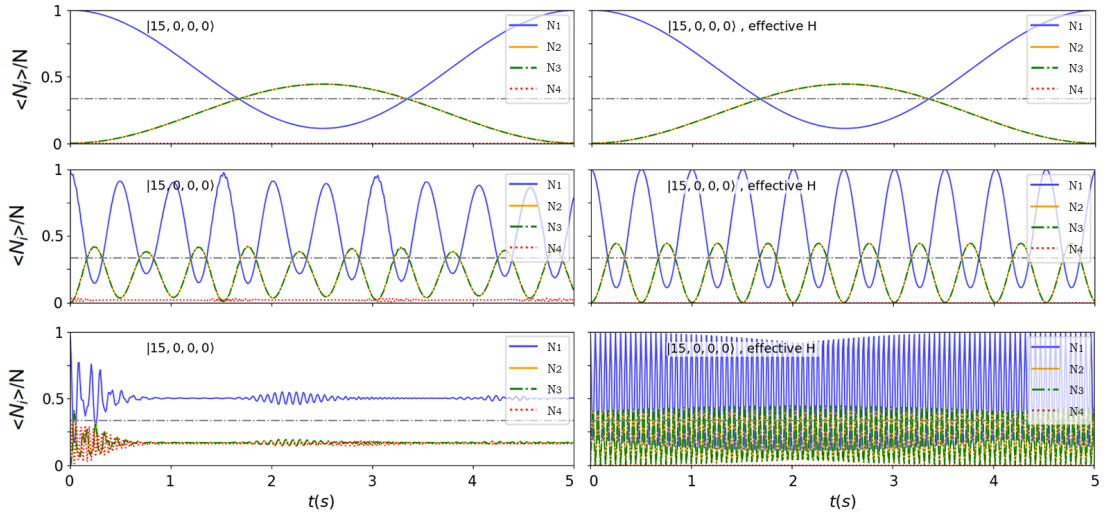

Figure 15: Dynamics in different regimes for the initial state $|15, 0, 0, 0\rangle$, using $H_{3,1}$ (left) and H_{eff} (right). The parameter $J/\hbar = 73.219$ Hz is fixed while the parameter U is varied. First row: $U/\hbar = 76.519$ Hz. Second row: $U/\hbar = 7.6519$ Hz. Third row: $U/\hbar = 0.76519$ Hz. The horizontal line marks $(N_1 + N_2 + N_3)/3$.

The energy bands for this model follow a similar pattern to those for the closed arrangement (see Figure 4), but now $M = N_1 + N_2 + N_3$ and $P = N_4$ and the vertical line divides the graph into the Rabi regime to the left of $\chi = 1$, where there are no clear bands, and the Josephson regime to the right of $\chi = 1$, where the resonance can be achieved.

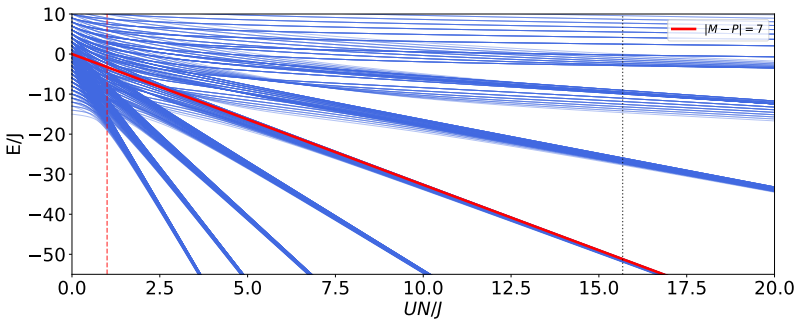

Figure 16: Energy bands for the open-configuration in the resonant regime with $N = 15$. Vertical lines at $\chi = 1$ (red), where the formation of bands starts, and $\chi = 15.676$, where $U/\hbar = 76.519$ Hz. The diagonal red line follows the equation: $E/J = -\chi(M - P)^2/N$, with $|M - P| = 7$.

The calculation of fidelity and entanglement follows the same procedure presented in the previous section (2.4 and 2.5). The visualization of the probability of selected Fock states in the open arrangement can be done using the method of histograms with indexes (see figure 5) or in a more concise way, using heat-maps (or 3D histograms) with fixed N_4 (since it remains constant in the resonant regime), setting N_1 and N_2 as the values of the x and y axis and the probability $|C_n|^2$ as the colour-coded z axis (see appendix D).

3.3 Interferometer

Four-well systems in the open-arrangement can also be used in interferometry. In this section we present a theoretical model of interferometer based on the schematic diagram below, which shows

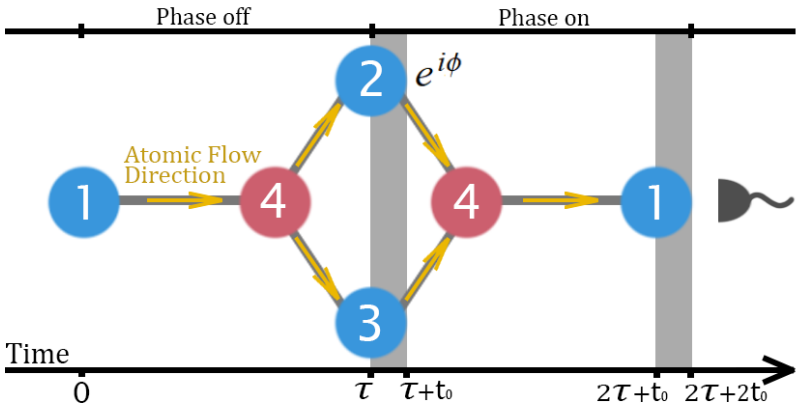

Figure 17: Schematic representation of the phase protocol. The dipolar atoms flow from well 1 to wells 2 and 3. We apply a break of integrability between τ and $\tau + t_0$, and $2\tau + t_0$ and $2\tau + 2t_0$, to implement the phase dependent term $e^{i\phi}$ acting on well 2 during the time interval in which the atoms are flowing back to the well 1. Subsequently, a measurement of the number of atoms in well 1 is performed in order to detect the constructive/destructive effects of interference.

To implement this interferometer, the hamiltonian (3.1.1) must be modified with a term for phase control acting in one of the wells, e.g. $a_2 \to e^{-i\phi}a_2$. Considering the initial state $|\Psi_0\rangle = |N, 0, 0, 0\rangle$ and the time-evolution:

$$|\Psi(t)\rangle = \mathcal{U}(t-\tau, \phi)\mathcal{U}(\tau, 0)|\Psi_0\rangle \tag{3.3.1}$$

$$\mathcal{U}(t, \phi) = \exp[-itH_{3,1}(\phi)/\hbar] \tag{3.3.2}$$

We let the system evolve with phase-shift zero until $\tau = \hbar\pi/(3J_{\text{eff}})$, when N_1 reaches its first minimum and the atomic current is maximally separated to occupy the wells 2 and 3. Then the phase is shifted by ϕ, the two atomic currents flow to well 4 and we observe the resulting interference in well 1 at 2τ, when N_1 would originally reach its maximum, as shown in figure 18 (regular dynamics with no phase-shift and once again using the same values for U, J and N for the purpose of comparison).

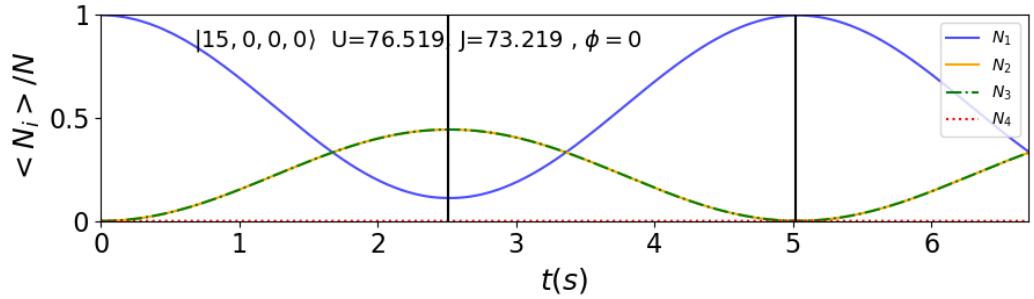

Figure 18: Dynamics of a system with $\phi = 0$. Vertical lines at τ and 2τ, respectively representing the moment where the phase ϕ would be altered and N_1 measured.

Now, by applying a phase shift, the expected value of $\langle N_1 \rangle / N$ varies greatly. Figure 19 shows the effects of $\phi = \pi$ in the dynamics, resulting in a minimum for $\langle N_1 \rangle / N$ at 2τ.

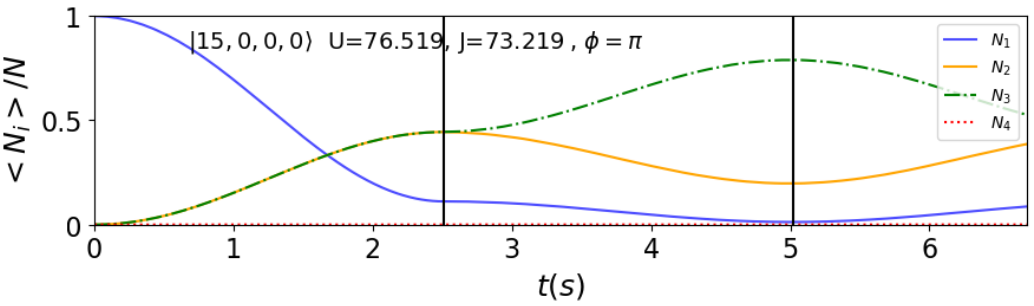

Figure 19: Dynamics for a system with $\phi = \pi$. Vertical lines at τ and 2τ.

The implementation of the phase and its effect on $\langle N_i \rangle$ are presented in the next subsection. Other open-arrangement dynamics, unrelated to the interferometer model, are shown in appendix D.

3.3.1 Phase Control Protocol

To implement the phase shift in a controllable way, we consider a new hamiltonian with a break term

$$H_b(\nu) = H_{3,1} - \nu \left(2N_2 - N_1 - N_3\right), \tag{3.3.3}$$

and the time evolution operator

$$\mathcal{U}(t, \nu) = \exp\left(-itH_b(\nu)/\hbar\right). \tag{3.3.4}$$

Thus, the phase control protocol (equivalent to (3.3.1)), is given by the following operations, in terms of the break parameter ν:

$$\begin{aligned} |\Psi(\nu)\rangle &= \mathcal{U}\left(t_0, \nu\right)\mathcal{U}(\tau, 0)\mathcal{U}\left(t_0, -\nu\right)\mathcal{U}(\tau, 0)|N, 0, 0, 0\rangle \\ &= \mathcal{U}_{\text{eff}}(\tau, \nu)\mathcal{U}(\tau, 0)|N, 0, 0, 0\rangle \end{aligned} \tag{3.3.5}$$

Where we defined the effective time evolution operator:

$$\mathcal{U}_{\text{eff}}(\tau,\nu) \equiv \mathcal{U}\left(t_0,\nu\right)\mathcal{U}(\tau,0)\mathcal{U}\left(t_0,-\nu\right). \tag{3.3.6}$$

In the resonant tunneling regime, for small t_0 in comparison with the typical time scale of the dynamics, we can consider the following approximation in terms of effective hamiltonian

$$\begin{aligned}\mathcal{U}\left(t_0,\pm\nu\right) &= \exp\left[-it_0H_{\text{eff}}/\hbar \pm it_0\nu\left(2N_2-N_1-N_3\right)/\hbar\right] \\ &\approx \exp\left[\pm it_0\nu\left(2N_2-N_1-N_3\right)/\hbar\right],\end{aligned} \tag{3.3.7}$$

since the dynamics is approximately frozen in the interval t_0, such that the hamiltonian H_{eff} has no effect and can be neglected. This leads to

$$\mathcal{U}_{\text{eff}}\left(\tau,\nu\right) = \exp\left(-i\tau H_{\text{eff}}\left(\nu\right)/\hbar\right), \tag{3.3.8}$$

which reproduces the analogous time evolution operator given in (3.3.2), with the phase dependent effective hamiltonian by identification (see details in appendix C)

$$\phi = 3\nu t_0/\hbar. \tag{3.3.9}$$

Observe, however, that the total protocol time is increased to $2\tau+2t_0$, in comparison to (3.3.1), due to the additional operations with the break of integrability to encode the phase.

The above protocol provides the interference pattern with high contrast (see appendix C for details)

$$\langle N_1(\phi)\rangle/N = \langle\Psi(\nu)\left|N_1\right|\Psi(\nu)\rangle/N = 1-\frac{80}{81}\sin^2(\phi/2), \quad \nu=\frac{\phi\hbar}{3t_0}. \tag{3.3.10}$$

The expected number of atoms in well 1 at 2τ can be plotted versus ϕ, as shown below

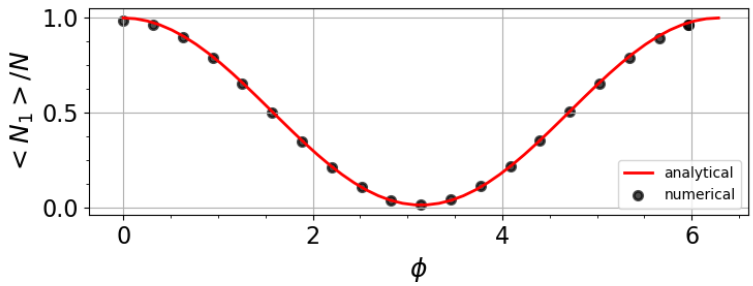

Figure 20: $\langle N_1\rangle/N$ distribution at $t=2\tau$ for different values of ϕ. Analytical results obtained using equation 3.3.10, numerical results obtained using equation 3.1.1.

The sensitivity of this model is also calculated in appendix C , yielding

$$\Delta\phi = \frac{\Delta N_1}{\left|\frac{d\langle N_1\rangle}{d\phi}\right|} = \frac{1}{N^{1/2}}\sqrt{1+\frac{1}{80}\sec^2(\phi/2)}. \tag{3.3.11}$$

Therefore, the interferometer has shot-noise limited sensitivity that scales with $1/\sqrt{N}$ [39], in contrast with the Heisenberg-limited closed model. The dependency on ϕ also implies that the sensitivity decreases for values of ϕ near π. Nevertheless, the model still achieves high contrast (see Eq.(3.3.10)) with an easily obtainable initial state $|N, 0, 0, 0\rangle$ and does not depend on the number of particles and whether its odd or even (unlike the results in (2.5.2) for the closed arrangement model).

3.3.2 Experimental Setup

The experimental setup for the interferometer is mathematically described in the appendix C. We use three sets of blue-detuned (tuned to a frequency above the resonant frequency) counter-propagating laser beams to create an optical lattice with the desired arrangement of wells. Its potential is given by

$$V_{\text{latt}}(x, y, \lambda) = -V_1 \sum_{j=1}^{3} \sin^2(kr \cdot u_j), \quad r = (x, y), \quad k = \frac{2\pi}{\lambda}, \tag{3.3.12}$$

where u_j are the vectors indicating the beams' directions.

Another counter-propagating laser beam, this time vertical and red-detuned (tuned to a frequency below the resonant frequency) is used to control the aspect ratio of the potential. Finally, a region with four potential wells is then isolated from the rest of the lattice using a vertical gaussian beam and the phase encoding is accomplished with the use of an off-center gaussian beam of weak intensity, shifting the potential and causing the integrability break.

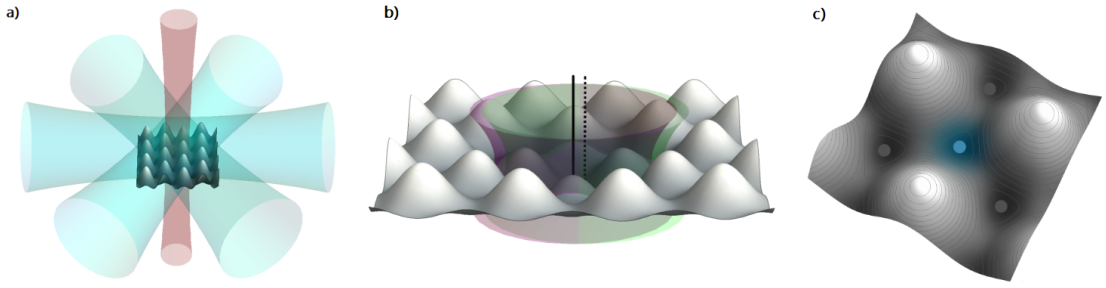

Figure 21: a) In cyan, three sets of counter-propagating beams separated by angles of $\pi/3$ radians create the optical lattice. In red, a vertical beam controls the aspect ratio of the potential. b) Another laser beam, shown in purple, is used to isolate a region with four wells (with the solid black line representing its z axis), and the beam used to control the integrability break and encode the phase is shown in green (off-center, with the dashed black line representing its z axis). c) The isolated four-well system with subspaces separated by colour

A top-down view of the four-well region is shown below, indicating the two positions of the green beam used to encode the phase on well 2 as described by the operators $\mathcal{U}(t_0, \nu)$ and $\mathcal{U}(t_0, -\nu)$.

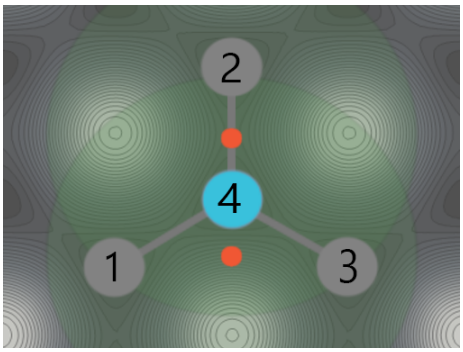

Figure 22: Top-down view of the isolated four-well system with subspaces separated by colour and the beam used to shift the potential and encode the phase shown in green in two different positions with its centers in red.

4 Conclusion

In this work we studied integrable models for systems with ultra-cold bosonic atoms in four potential wells linked by quantum tunneling. Two cases were analyzed: the closed arrangement, where there are two wells in each class, and the open arrangement, with three wells in one class and one in the other. Both cases had their hamiltonians presented and dynamics studied, mainly in resonant regimes, where the effective hamiltonian and the interferometer protocols are valid. Numerical and computational methods were applied to generate the simulations (using the matrix representation shown in appendix A) and diagrams throughout this work.

In chapter two the closed arrangement was introduced and explained in the context of the different possible regimes dependent on the parameters chosen. In the resonant regime, we saw that the number of bosons in each subspace is constant and there is the formation of energy bands. The Fock state distribution was analyzed in the particular case where an Uber-NOON state is formed (in systems with odd N) with high fidelity, also causing a drop in the entanglement parameter. In the final subsection, the protocols for an interferometer were presented (based on existing research).

Having shown known results in chapter 2, chapter 3 analyses the open arrangement in a similar way, (utilizing the same parameters for the sake of comparison, see figures 3 and 15). We noted that in the open arrangement subspace B only contains well 4, reflecting in a constant number of bosons in this well in the resonant regime and the omission of a_4 and $a_4^\dagger$ in the effective hamiltonian, derived in appendix B. Finally, an original protocol for an open-arrangement interferometer is proposed, along with a brief explanation of a possible experimental setup (described mathematically in appendix C).

The interferometer models presented in this work have different limits in sensitivity due to the differences in the geometry of each system and the initial states used. The closed-arrangement interferometer is able to achieve Heisenberg-limited sensitivity due to the carefully prepared NOON state gate, while the open-arrangement interferometer only achieves shot-noise limited sensitivity, but on the other hand, requires a simpler initial state, with all particles initially in well 1, and has high contrast for any N.

The results obtained reaffirm the four-well quantum tunneling models' distinct physical properties and possible applications in quantum metrology. Optimal values for the parameters to be used in the open-arrangement interferometer are yet to be obtained and since the protocols for the formation of the NOON state are specific to the closed arrangement, further research is needed to propose a new initial state or configuration to improve the sensitivity limit of the open-arrangement model (for this purpose, the different open-arrangement dynamics shown in appendix D may be useful).

A Matrix Representation of Hamiltonians

In order to facilitate the obtainment of eigenvectors and eigenvalues, we can represent hamiltonians as matrices with the following basis:

$$\mathfrak{B} = \{|N, ..., 0, ..., 0\rangle, \cdots, |0, ..., N, ..., 0\rangle, \cdots, |0, ..., 0, ..., N\rangle\}$$

Thus, the hamiltonian can be written as:

$$[H_{n,m}] = \begin{pmatrix} \langle N, ..., 0, ..., 0|H_{n,m}|N, ..., 0, ..., 0\rangle & \cdots & \langle 0, ..., 0, ..., N|H_{n,m}|N, ..., 0, ..., 0\rangle \\ \vdots & \ddots & \vdots \\ \langle N, ..., 0, ..., 0|H_{n,m}|0, ..., 0, ..., N\rangle & \cdots & \langle 0, ..., 0, ..., N|H_{n,m}|0, ..., 0, ..., N\rangle \end{pmatrix} \tag{A.0.1}$$

This representation is not unique and can be used for any N. The calculation of the matrix elements is done applying the following relations (shown for $N = 2$):

$$\begin{gathered} a_1^\dagger a_2|n_1, n_2\rangle = \sqrt{n_2}a_1^\dagger|n_1, n_2 - 1\rangle = \sqrt{n_2(n_1 + 1)}|n_1 + 1, n_2 - 1\rangle \\ a_2^\dagger a_1|n_1, n_2\rangle = \sqrt{n_1}a_2^\dagger|n_1 - 1, n_2\rangle = \sqrt{n_1(n_2 + 1)}|n_1 - 1, n_2 + 1\rangle \\ N_1|n_1, n_2\rangle = a_1^\dagger a_1|n_1, n_2\rangle = n_1|n_1, n_2\rangle \\ N_2|n_1, n_2\rangle = a_2^\dagger a_2|n_1, n_2\rangle = n_2|n_1, n_2\rangle \end{gathered}$$

Applying this method on the closed 4-well hamiltonian yields:

$$\begin{gathered} \langle N_1', N_2', N_3', N_4'|H_{2,2}|N_1, N_2, N_3, N_4\rangle = \\ [U(N_1 - N_2 + N_3 - N_4)^2]\delta_{N_1',N_1}\delta_{N_2',N_2}\delta_{N_3',N_3}\delta_{N_4',N_4} - (J/2)[\\ (\sqrt{N_1(N_2 + 1)}\delta_{N_1',N_1-1}\delta_{N_2',N_2+1} + \sqrt{N_2(N_1 + 1)}\delta_{N_1',N_1+1}\delta_{N_2',N_2-1})\delta_{N_3',N_3}\delta_{N_4',N_4} + \\ (\sqrt{N_2(N_3 + 1)}\delta_{N_2',N_2-1}\delta_{N_3',N_3+1} + \sqrt{N_3(N_2 + 1)}\delta_{N_2',N_2+1}\delta_{N_3',N_3-1})\delta_{N_1',N_1}\delta_{N_4',N_4} + \\ (\sqrt{N_3(N_4 + 1)}\delta_{N_3',N_3-1}\delta_{N_4',N_4+1} + \sqrt{N_4(N_3 + 1)}\delta_{N_3',N_3+1}\delta_{N_4',N_4-1})\delta_{N_1',N_1}\delta_{N_2',N_2} + \\ (\sqrt{N_4(N_1 + 1)}\delta_{N_4',N_4-1}\delta_{N_1',N_1+1} + \sqrt{N_1(N_4 + 1)}\delta_{N_4',N_4+1}\delta_{N_1',N_1-1})\delta_{N_2',N_2}\delta_{N_3',N_3}] \end{gathered} \tag{A.0.2}$$

Where δ is the Kronecker delta.

Similarly, for the open 4-well hamiltonian:

$$\begin{gathered} \langle N_1', N_2', N_3', N_4'|H_{3,1}|N_1, N_2, N_3, N_4\rangle = \\ [U(N_1 + N_2 + N_3 - N_4)^2]\delta_{N_1',N_1}\delta_{N_2',N_2}\delta_{N_3',N_3}\delta_{N_4',N_4} - (J/\sqrt{3})[\\ (\sqrt{N_1(N_4 + 1)}\delta_{N_1',N_1-1}\delta_{N_4',N_4+1} + \sqrt{N_4(N_1 + 1)}\delta_{N_1',N_1+1}\delta_{N_4',N_4-1})\delta_{N_3',N_3}\delta_{N_2',N_2} + \\ (\sqrt{N_2(N_4 + 1)}\delta_{N_2',N_2-1}\delta_{N_4',N_4+1} + \sqrt{N_4(N_2 + 1)}\delta_{N_2',N_2+1}\delta_{N_4',N_4-1})\delta_{N_1',N_1}\delta_{N_3',N_3} + \\ (\sqrt{N_3(N_4 + 1)}\delta_{N_3',N_3-1}\delta_{N_4',N_4+1} + \sqrt{N_4(N_3 + 1)}\delta_{N_3',N_3+1}\delta_{N_4',N_4-1})\delta_{N_1',N_1}\delta_{N_2',N_2}] \end{gathered} \tag{A.0.3}$$

B Effective Hamiltonian Calculations

In the resonant tunneling regime the bosons tend to be restricted to their respective classes, thus, we can consider second-order tunneling processes to obtain effective hamiltonians. In the following subsections we obtain expressions for the closed and open arrangement.

Four-Well Closed Arrangement

The hamiltonian for the Four-Well model in Closed Arrangement can be written as:

$$\begin{aligned} H_{2,2} &= H_0 + H_1 \\ H_0 &= -U(N_1 - N_2 + N_3 - N_4)^2 \\ H_1 &= \frac{J}{2}[(a_1^\dagger + a_3^\dagger)(a_2 + a_4) + (a_2^\dagger + a_4^\dagger)(a_1 + a_3)] \end{aligned} \tag{B.0.1}$$

For the inital condition $|M-l, P-k, l, k\rangle, l = 0, ..., M; k = 0, ..., P; P = 0, ..., N$ and $N = M + P$ (total number of bosons), we obtain:

$$\therefore H_0|\Psi\rangle = U(N-2P)^2|\Psi\rangle \tag{B.0.2}$$

In order to determine the effective hamiltonian we utilize time-dependent perturbation theory for the transitions, as follows:

$$\begin{aligned} &H_1|N-P-l, P-k, l, k\rangle = \\ &\quad\frac{J}{2}(\sqrt{(N-P-l)(P-k+1)}|N-P-l-1, P-k+1, l, k\rangle \\ &\quad+ \sqrt{(N-P-l)(k+1)}|N-P-l-1, P-k, l, k+1\rangle \\ &\quad+ \sqrt{(N-P-l+1)(P-k)}|N-P-l+1, P-k-1, l, k\rangle \\ &\quad+ \sqrt{(N-P-l+1)k}|N-P-l+1, P-k, l, k-1\rangle \\ &\quad+ \sqrt{(P-k)(l+1)}|N-P-l, P-k-1, l+1, k\rangle \\ &\quad+ \sqrt{(P-k+1)l}|N-P-l, P-k+1, l-1, k\rangle \\ &\quad+ \sqrt{l(k+1)}|N-P-l, P-k, l-1, k+1\rangle \\ &\quad+ \sqrt{(l+1)k}|N-P-l, P-k, l+1, k-1\rangle) \end{aligned} \tag{B.0.3}$$

$$
\begin{aligned}
&H_1|N-P-l-1,P-k,l+1,k\rangle = \\
&\quad\frac{J}{2}(\sqrt{(N-P-l-1)(P-k+1)}|N-P-l-2,P-k+1,l+1,k\rangle \\
&\quad+\sqrt{(N-P-l-1)(k+1)}|N-P-l-2,P-k,l+1,k+1\rangle \\
&\quad+\sqrt{(N-P-l)(P-k)}|N-P-l,P-k-1,l+1,k\rangle \\
&\quad+\sqrt{(N-P-l)k}|N-P-l,P-k,l+1,k-1\rangle \\
&\quad+\sqrt{(P-k)(l+2)}|N-P-l-1,P-k-1,l+2,k\rangle \\
&\quad+\sqrt{(P-k+1)(l+1)}|N-P-l-1,P-k+1,l,k\rangle \\
&\quad+\sqrt{(l+2)k}|N-P-l-1,P-k,l+2,k-1\rangle \\
&\quad+\sqrt{(l+1)(k+1)}|N-P-l-1,P-k,l,k+1\rangle)
\end{aligned}
\tag{B.0.4}
$$

$$
\begin{aligned}
&H_1|N-P-l,P-k-1,l,k+1\rangle = \\
&\quad\frac{J}{2}(\sqrt{(N-P-l)(P-k)}|N-P-l-1,P-k,l,k+1\rangle \\
&\quad+\sqrt{(N-P-l)(k+2)}|N-P-l-1,P-k-1,l,k+2\rangle \\
&\quad+\sqrt{(N-P-l+1)(P-k-1)}\mid N-P-l+1,P-k-2,l,k+1 \\
&\quad+\sqrt{(N-P-l+1)(k+1)}|N-P-l+1,P-k-1,l,k\rangle \\
&\quad+\sqrt{(P-k-1)(l+1)}|N-P-l,P-k-2,l+1,k+1\rangle \\
&\quad+\sqrt{(P-k)l|N-P-l,P-k,l-1,k+1\rangle} \\
&\quad+\sqrt{l(k+2)|N-P-l,P-k-1,l-1,k+2\rangle} \\
&\quad+\sqrt{(l+1)(k+1)}|N-P-l,P-k-1,l+1,k\rangle)
\end{aligned}
\tag{B.0.5}
$$

Using the formula for second order processes:

$$
V^{(2)}=\sum_{s\in\Lambda_k}\frac{H|s\rangle\langle s|H}{E_i-E_s} \tag{B.0.6}
$$

Where Λ_k is a set of intermediate states. The transition rate is given by:

$$
T_{i\to j}(k)=\langle f|V^{(2)}|i\rangle \tag{B.0.7}
$$

Thus, we obtain:

$$
\begin{aligned}
&\langle N-P-l-1,P-k,l+1,k\,|H_{\text{eff}}|\,N-P-l,P-k,l,k\rangle \\
&\quad=\frac{J^2}{4U}\left(\frac{(P-k)\sqrt{(N-P-l)(l+1)}+k\sqrt{(N-P-l)(l+1)}}{4(N-2P+1)}\right) \\
&\qquad-\frac{J^2}{4U}\left(\frac{(P-k+1)\sqrt{(N-P-l)(l+1)}+(k+1)\sqrt{(N-P-l)(l+1)}}{4(N-2P-1)}\right) \\
&\qquad=\frac{J^2}{16U}\left(\frac{P}{N-2P+1}-\frac{P+2}{N-2P-1}\right)\sqrt{(N-P-l)(l+1)}
\end{aligned}
\tag{B.0.8}
$$

$$
\begin{aligned}
&\langle N-P-l, P-k-1, l, k+1 \,|H_{\text{eff}}|\, N-P-l, P-k, l, k\rangle \\
&\quad = \frac{J^2}{4U}\left(\frac{(l+1)\sqrt{(P-k)(k+1)}+(N-P-l+1)\sqrt{(P-k)(k+1)}}{4(N-2P+1)}\right) \\
&\qquad - \frac{J^2}{4U}\left(\frac{(N-P-l)\sqrt{(P-k)(k+1)}+l\sqrt{(P-k)(k+1)}}{4(N-2P-1)}\right) \\
&\quad = \frac{J^2}{16U}\left(\frac{N-P+2}{N-2P+1}-\frac{N-P}{N-2P-1}\right)\sqrt{(P-k)(k+1)}
\end{aligned}
\tag{B.0.9}
$$

$$
\begin{aligned}
&\langle N-P-l+1, P-k-1, l-1, k+1 \,|H_{\text{eff}}|\, N-P-l, P-k, l, k\rangle \\
&\quad = \frac{J^2}{4U}\left(\frac{\sqrt{(N-P-l+1)(P-k)l(k+1)}}{4(N-2P+1)}\right) \\
&\qquad - \frac{J^2}{4U}\left(\frac{\sqrt{(N-P-l+1)(P-k)l(k+1)}}{4(N-2P-1)}\right) \\
&\quad = \frac{J^2}{16U}\left(\frac{1}{N-2P+1}-\frac{1}{N-2P-1}\right)\sqrt{(N-P-l+1)(P-k)l(k+1)}
\end{aligned}
\tag{B.0.10}
$$

Therefore:

$$
\begin{aligned}
H_{\text{eff}} = &\frac{J^2}{16U}\left(\frac{P}{N-2P+1}-\frac{P+2}{N-2P-1}\right)(a_1^\dagger a_3 + a_3^\dagger a_1) \\
&+ \frac{J^2}{16U}\left(\frac{N-P+2}{N-2P+1}-\frac{N-P}{N-2P-1}\right)(a_2^\dagger a_4 + a_4^\dagger a_2) \\
&+ \frac{J^2}{16U}\left(\frac{1}{N-2P+1}-\frac{1}{N-2P-1}\right) \\
&(a_1^\dagger a_2 a_3 a_4^\dagger + a_1^\dagger a_2^\dagger a_3 a_4 + a_1 a_2^\dagger a_3^\dagger a_4 + a_1 a_2 a_3^\dagger a_4^\dagger)
\end{aligned}
\tag{B.0.11}
$$

Or, in terms of its conserved operators [26] , up to a constant:

$$
\begin{aligned}
H_{\text{eff}} &= (N+1)\Omega(Q_1+Q_2) - 2\Omega Q_1 Q_2 \\
\Omega &= J^2/(4U((M-P)^2-1)) \\
Q_1 &= \frac{1}{2}(N_1+N_3-a_1^\dagger a_3 - a_3^\dagger a_1) \\
Q_2 &= \frac{1}{2}(N_2+N_4-a_2^\dagger a_4 - a_4^\dagger a_2)
\end{aligned}
\tag{B.0.12}
$$

Four-Well Open Arrangement

The hamiltonian for the Four-Well model in Open Arrangement can be written as:

$$
H_{3,1} = H_0 + H_1
$$

$$
H_0 = -U(N_1+N_2+N_3-N_4)^2 \tag{B.0.13}
$$

$$
H_1 = -\frac{J}{\sqrt{3}}[(a_1^\dagger + a_2^\dagger + a_3^\dagger)a_4 + a_4^\dagger(a_1+a_2+a_3))] \tag{B.0.14}
$$

Once again, using the equations B.0.6 and B.0.7, we obtain:

$$T_{i\to j}(1) = \frac{J^2\sqrt{1+k}(1+N)\sqrt{-k-l+N-P}}{12(-1+N-2P)(1+N-2P)U} \tag{B.0.15}$$

$$|i\rangle = |-k-l+N-P,k,l,P\rangle, \quad |f\rangle = |-1-k-l+N-P,1+k,l,P\rangle$$

$$\Lambda_1 = \{|-1-k-l+N-P,k,l,1+P\rangle, |-k-l+N-P,1+k,l,-1+P\rangle\}$$

$$T_{i\to j}(2) = \frac{J^2\sqrt{1+1}(1+N)\sqrt{-k-1+N-P}}{12(-1+N-2P)(1+N-2P)U} \tag{B.0.16}$$

$$|i\rangle = |-k-1+N-P,k,1,P\rangle, \quad |f\rangle = |-1-k-1+N-P,k,1+1,P\rangle$$

$$\Lambda_2 = \{|-1-k-1+N-P,k,1,1+P\rangle, \quad |-k-1+N-P,k,1+1,-1+P\rangle\}$$

$$T_{i\to j}(3) = \frac{J^2\sqrt{k}(1+N)\sqrt{1-k-1+N-P}}{12(-1+N-2P)(1+N-2P)U} \tag{B.0.17}$$

$$|i\rangle = |-k-1+N-P,k,1,P\rangle, \quad |f\rangle = |1-k-1+N-P,-1+k,1,P\rangle$$

$$\Lambda_3 = \{|-k-1+N-P,-1+k,1,1+P\rangle, \quad |1-k-1+N-P,k,1,-1+P\rangle\}$$

$$T_{i\to j}(4) = \frac{J^2\sqrt{k}\sqrt{1+1}(1+N)}{12(-1+N-2P)(1+N-2P)U} \tag{B.0.18}$$

$$|i\rangle = |-k-1+N-P,k,1,P\rangle, \quad |f\rangle = |-k-1+N-P,-1+k,1+1,P\rangle$$

$$\Lambda_4 = \{|-k-1+N-P,-1+k,1,1+P\rangle, \quad |-k-1+N-P,k,1+1,-1+P\rangle\}$$

$$T_{i\to j}(5) = \frac{J^2\sqrt{1}(1+N)\sqrt{1-k-1+N-P}}{12(-1+N-2P)(1+N-2P)U} \tag{B.0.19}$$

$$|i\rangle = |-k-1+N-P,k,1,P\rangle, \quad |f\rangle = |1-k-1+N-P,k,-1+1,P\rangle$$

$$\Lambda_5 = \{ \quad |-k-1+N-P,k,-1+1,1+P\rangle, \quad |1-k-1+N-P,k,1,-1+P\rangle\}$$

$$T_{i\to j}(6) = \frac{J^2\sqrt{1+k}\sqrt{1}(1+N)}{12(-1+N-2P)(1+N-2P)U} \tag{B.0.20}$$

$$|i\rangle = |-k-1+N-P,k,1,P\rangle, \quad |f\rangle = |-k-1+N-P,1+k,-1+1,P\rangle$$

$$\Lambda_6 = \{|-k-1+N-P,k,-1+1,1+P\rangle, \quad |-k-1+N-P,1+k,1,-1+P\rangle\}$$

Therefore we can write the following effective hamiltonian:

$$H_{\text{eff}} = J_{\text{eff}}[(a_1^\dagger a_2 + a_2^\dagger a_1) + (a_1^\dagger a_3 + a_3^\dagger a_1) + (a_2^\dagger a_3 + a_3^\dagger a_2)] \tag{B.0.21}$$

$$J_{\text{eff}} = \frac{J^2(N+1)}{12U(N-2P-1)(N-2P+1)} \tag{B.0.22}$$

C Calculations for the Interferometers

In this appendix we present relevant calculations for the closed and open interferometer models, such as the derivation of the sensitivity (and therefore contrast). We also calculate τ and $\mathcal{U}_{\text{eff}}$ and give a mathematical description of the experimental setup proposed for the open-arrangement interferometer. (Calculations made using $\hbar = 1$ for simplicity.)

Four-Well Closed Arrangement Sensitivity

Using the simplified notation: $\langle O \rangle = \langle \Psi(N, P, \phi) | O | \Psi(N, P, \phi) \rangle$, we obtain the following relations for the closed arrangement:

$$\begin{aligned} \left\langle (N_1 - N_3)^2 \right\rangle &= \left\langle N_1^2 \right\rangle + \left\langle N_3^2 \right\rangle - 2 \left\langle N_1 N_3 \right\rangle \\ \left\langle (N_1 + N_3)^2 \right\rangle &= \left\langle N_1^2 \right\rangle + \left\langle N_3^2 \right\rangle + 2 \left\langle N_1 N_3 \right\rangle = (N - P)^2 \end{aligned} \tag{C.0.1}$$

From the equations above, we see that:

$$\begin{aligned} \left\langle N_1^2 \right\rangle + \left\langle N_3^2 \right\rangle &= \frac{1}{2} \left\langle (N_1 - N_3)^2 \right\rangle + \frac{1}{2}(N - P)^2 \\ \left\langle N_1^2 \right\rangle - \left\langle N_3^2 \right\rangle &= \left\langle (N_1 + N_3)(N_1 - N_3) \right\rangle = (N - P) \left\langle N_1 - N_3 \right\rangle \end{aligned} \tag{C.0.2}$$

Thus:

$$\left\langle N_3^2 \right\rangle = \frac{1}{4} \left\langle (N_1 - N_3)^2 \right\rangle + \frac{1}{4}(N - P)^2 - \frac{1}{2}(N - P) \left\langle N_1 - N_3 \right\rangle \tag{C.0.3}$$

And since

$$\begin{aligned} \langle N_3 \rangle &= \frac{1}{2} \langle N_1 + N_3 \rangle - \frac{1}{2} \langle N_1 - N_3 \rangle = \frac{1}{2}(N - P) - \frac{1}{2} \langle N_1 - N_3 \rangle \\ \langle N_3 \rangle^2 &= \frac{1}{4} \left[(N - P)^2 + \langle N_1 - N_3 \rangle^2 - 2(N - P) \langle N_1 - N_3 \rangle \right] \end{aligned} \tag{C.0.4}$$

We obtain

$$\begin{aligned} (\Delta N_3)^2 =& \left\langle N_3^2 \right\rangle - \langle N_3 \rangle^2 \\ =& \frac{1}{4} \left\langle (N_1 - N_3)^2 \right\rangle + \frac{1}{4}(N - P)^2 - \frac{1}{2}(N - P) \left\langle N_1 - N_3 \right\rangle \\ & - \frac{1}{4} \left[(N - P)^2 + \langle N_1 - N_3 \rangle^2 - 2(N - P) \langle N_1 - N_3 \rangle \right] \end{aligned} \tag{C.0.5}$$

Thus,

$$(\Delta N_3)^2 = \left\langle N_3^2 \right\rangle - \langle N_3 \rangle^2 = \frac{1}{4} \left\langle (N_1 - N_3)^2 \right\rangle - \frac{1}{4} \langle N_1 - N_3 \rangle^2 . \tag{C.0.6}$$

For $t_m = \pi / 2\Omega$ and N odd, we find

$$\begin{aligned} \langle N_1 - N_3 \rangle &= (-1)^{(N+1)/2} (N - P) \cos \phi \\ \left\langle (N_1 - N_3)^2 \right\rangle &= (N - P)^2 \end{aligned} \tag{C.0.7}$$

Thus,

$$\Delta N_3 = \frac{1}{2}(N-P)|\sin\phi|,$$
$$\langle N_3\rangle = (N-P)\frac{1}{2}\left(1-(-1)^{(N+1)/2}\cos\phi\right) = (N-P)\cos^2\left(\phi/2-\left[1+(-1)^{(N+1)/2}\right]\frac{\pi}{4}\right) \tag{C.0.8}$$

For $\phi = P\varphi$, we find the sensitivity of the interferometer:

$$\Delta\varphi = \frac{\Delta N_3}{\left|\frac{d\langle N_3\rangle}{d\varphi}\right|} = \frac{1}{P} \tag{C.0.9}$$

For initial state

$$|\Psi(N, N-P, (N-P)\varphi)\rangle = \frac{1}{\sqrt{2}}\left(|P, N-P, 0, 0\rangle + e^{i(N-P)\varphi}|P, 0, 0, N-P\rangle\right)$$

The system achieves Heisenberg-limited phase sensitivity, since

$$\Delta\varphi = \frac{1}{N-P} = \frac{1}{M} \tag{C.0.10}$$

Four-Well Open Arrangement $\mathcal{U}_{\text{eff}}$ Operator

The approximation made in eq.3.3.8 leads to:

$$\begin{aligned}\mathcal{U}_{\text{eff}}(\tau,\nu) &= \mathcal{U}(t_0,\nu)\,\mathcal{U}(\tau,0)\mathcal{U}(t_0,-\nu)\\ &\approx e^{it_0\nu\tau(2N_2-N_1-N_3)}e^{-i\tau H_{\text{eff}}}e^{-it_0\nu(2N_2-N_1-N_3)}\\ &= \exp\left(-i\tau e^{i\nu t_0(2N_2-N_1-N_3)}H_{\text{eff}}e^{-i\nu t_0(2N_2-N_1-N_3)}\right)\end{aligned} \tag{C.0.11}$$

Rewriting the effective hamiltonian in the form

$$H_{\text{eff}} = J_{\text{eff}}\,\mathcal{T} \tag{C.0.12}$$

With the operators

$$\mathcal{T} = 2R_+ + 2S, \quad R_\pm = \frac{a_2^\dagger a_{13} \pm a_{13}^\dagger a_2}{\sqrt{2}}, \quad a_{13} = \frac{a_1+a_3}{\sqrt{2}}, \quad S = \frac{a_1^\dagger a_3 + a_3^\dagger a_1}{2} \tag{C.0.13}$$

Which satisfy the commutation relations

$$[2N_2-N_1-N_3, R_\pm] = 3R_\mp, \quad [2N_2-N_1-N_3, S] = 0 \tag{C.0.14}$$

One can show that

$$e^{i\theta(2N_2-N_1-N_3)}\mathcal{T}e^{-i\theta(2N_2-N_1-N_3)} = 2i\sin(3\theta)R_- + 2\cos(3\theta)R_+ + 2S \tag{C.0.15}$$

Using the above expression, we obtain

$$\begin{aligned}H_{\text{eff}}(\nu) &\equiv e^{i\nu t_0(2N_2-N_1-N_3)}H_{\text{eff}}e^{-i\nu t_0(2N_2-N_1-N_3)}\\ &= J_{\text{eff}}\left[e^{i3\nu t_0}a_2^\dagger(a_1+a_3) + e^{-i3\nu t_0}a_2^\dagger\left(a_1^\dagger+a_3^\dagger\right) + a_1^\dagger a_3 + a_3^\dagger a_1\right]\end{aligned} \tag{C.0.16}$$

This leads to:

$$\mathcal{U}_{\text{eff}}(\tau,\nu) = \exp\left(-i\tau H_{\text{eff}}(\nu)\right) \tag{C.0.17}$$

And we identify the relation between the parameter ν and the phase ϕ, which is given by

$$\phi = 3\nu t_0 \tag{C.0.18}$$

Four-Well Open Arrangement Tau and Sensitivity

To obtain the value used for τ, we start with the effective hamiltonian written as:

$$\begin{aligned} H_{\text{eff}} &= J_{\text{eff}}\left(a_1^\dagger a_2 + a_2^\dagger a_1 + a_1^\dagger a_3 + a_3^\dagger a_1 + a_2^\dagger a_3 + a_3^\dagger a_2\right) \\ &= 2J_{\text{eff}}A_+ + J_{\text{eff}}\left(N_a - N_b\right) \end{aligned} \tag{C.0.19}$$

Where we define:

$$\begin{aligned} a_{23} &= \frac{a_2 + a_3}{\sqrt{2}} \quad , \quad b_{23} = \frac{a_2 - a_3}{\sqrt{2}} \quad , \quad N_a = a_{23}^\dagger a_{23} \quad , \quad N_b = b_{23}^\dagger b_{23} \\ A_\pm &= \frac{a_1^\dagger a_{23} \pm a_{23}^\dagger a_1}{\sqrt{2}} \end{aligned} \tag{C.0.20}$$

And the number of particles in well 1 is given by:

$$N_1(t) = e^{-itH_{\text{eff}}} N_1 e^{itH_{\text{eff}}} = N_1 + (-it)\left[H_{\text{eff}}, N_1\right] + \frac{(-it)^2}{2!}\left[H_{\text{eff}}, \left[H_{\text{eff}}, N_1\right]\right] + \cdots \tag{C.0.21}$$

Where the identity $e^Q P e^{-Q} = P + [Q,P] + \frac{1}{2!}[Q,[Q,P]] + \cdots$ was used.
Now, the commutation relations

$$\begin{aligned} &[N_a, A_\pm] = -A_\mp \quad , \quad [N_b, A_\pm] = 0 \quad , \quad [A_+, A_-] = N_a - N_1 \quad , \quad [N_a, N_b] = 0 \\ &\left[N_b, a_{23}^\dagger\right] = 0 \quad , \quad [N_b, a_{23}] = 0 \quad , \quad [N_a, a_{23}] = -a_{23} \quad , \quad \left[N_a, a_{23}^\dagger\right] = a_{23}^\dagger \end{aligned} \tag{C.0.22}$$

Lead us to:

$$\begin{aligned} \left[H_{\text{eff}}, N_1\right] &= -2J_{\text{eff}}A_- \\ \left[H_{\text{eff}}, A_-\right] &= 2J_{\text{eff}}\left(N_a - N_1\right) - J_{\text{eff}}A_+ \equiv \Gamma, \\ \left[H_{\text{eff}}, \Gamma\right] &= 9J_{\text{eff}}^2 A_- \end{aligned} \tag{C.0.23}$$

And we obtain

$$\begin{aligned} N_1(t) =& N_1 + (-2J_{\text{eff}})\left[(-it) + \frac{(-it)^3}{3!}\left(9J_{\text{eff}}^2\right) + \frac{(-it)^5}{5!}\left(9J_{\text{eff}}^2\right)^2 + \cdots\right] A_- \\ &+ (-2J_{\text{eff}})\left[\frac{(-it)^2}{2!} + \frac{(-it)^4}{4!}\left(9J_{\text{eff}}^2\right) + \frac{(-it)^6}{6!}\left(9J_{\text{eff}}^2\right)^2 + \cdots\right]\Gamma \end{aligned} \tag{C.0.24}$$

Therefore,

$$N_1(t) = N_1 + \frac{2}{3} i \sin\left(3J_{\text{eff}} t\right) A_- + \frac{4}{9} \sin^2\left(\frac{3}{2} J_{\text{eff}} t\right) \left[2\left(N_a - N_1\right) - A_+\right] \tag{C.0.25}$$

$$\frac{\langle N_1 \rangle}{N} = \frac{1}{N} \left\langle N,0,0,0 \left| e^{-itH_{\text{eff}}} N_1 e^{itH_{\text{eff}}} \right| N,0,0,0 \right\rangle = 1 - \frac{8}{9} \sin^2\left(\frac{3}{2} J_{\text{eff}} t\right) \tag{C.0.26}$$

And the condition $\frac{3}{2} J_{\text{eff}} \tau = \frac{\pi}{2}$, yields

$$\tau = \frac{\pi}{3J_{\text{eff}}} \tag{C.0.27}$$

Upon making the transformation $a_2 \to e^{-i\phi} a_2$ in the hamiltonian, we obtain

$$\begin{aligned} \tilde{N}_1(\tau) &= e^{-i\tau H_{\text{eff}}} N_1 e^{i\tau H_{\text{eff}}}\big|_{a_2 \to e^{-i\phi} a_2} = N_1(\tau)\big|_{a_2 \to e^{-i\phi} a_2} \\ &= N_1 + \frac{2}{3} i \sin\left(3J_{\text{eff}} \tau\right) \tilde{A}_- + \frac{4}{9} \sin^2\left(\frac{3}{2} J_{\text{eff}} \tau\right) \left[2\left(\tilde{N}_a - N_1\right) - \tilde{A}_+\right] \end{aligned} \tag{C.0.28}$$

Where we define the operators

$$\begin{aligned} &\tilde{a}_{23} = \frac{e^{-i\phi} a_2 + a_3}{\sqrt{2}} = a_{23} + \lambda a_2, \quad \tilde{a}_{23}^\dagger = \frac{e^{i\phi} a_2^\dagger + a_3^\dagger}{\sqrt{2}} = a_{23}^\dagger + \lambda^* a_2^\dagger, \quad \lambda = \frac{e^{-i\phi} - 1}{\sqrt{2}} \\ &\tilde{N}_a = \tilde{a}_{23}^\dagger \tilde{a}_{23} = N_a + \frac{1}{\sqrt{2}} \tau_{23}, \quad \tau_{23} = \lambda^* a_2^\dagger a_3 + \lambda a_3^\dagger a_2 \\ &\tilde{A}_\pm = \frac{a_1^\dagger \tilde{a}_{23} \pm \tilde{a}_{23}^\dagger a_1}{\sqrt{2}} = A_\pm + \frac{1}{\sqrt{2}} \tau_\pm, \quad \tau_\pm = \lambda a_1^\dagger a_2 \pm \lambda^* a_2^\dagger a_1 \end{aligned} \tag{C.0.29}$$

The, eq.(C.0.19) can be rewritten as

$$\tilde{N}_1(\tau) = N_1(\tau) + \Lambda \tag{C.0.30}$$

Where we define

$$\begin{aligned} \Lambda &= \frac{2}{3} i \sin\left(3J_{\text{eff}} \tau\right) \frac{1}{\sqrt{2}} \tau_- + \frac{4}{9} \sin^2\left(\frac{3}{2} J_{\text{eff}} \tau\right) \left(\sqrt{2} \tau_{23} - \frac{1}{\sqrt{2}} \tau_+\right) \\ &= \frac{4}{9} \left(\sqrt{2} \tau_{23} - \frac{1}{\sqrt{2}} \tau_+\right) \end{aligned} \tag{C.0.31}$$

Thus,

$$e^{-i\tau H_{\text{eff}}} \tilde{N}_1(\tau) e^{i\tau H_{\text{eff}}} = N_1(2\tau) + e^{-i\tau H_{\text{eff}}} \Lambda e^{i\tau H_{\text{eff}}}. \tag{C.0.32}$$

Since

$$\lambda + \lambda^* = -2\sqrt{2} \sin^2(\phi/2), \quad \lambda - \lambda^* = -i\sqrt{2} \sin\phi \tag{C.0.33}$$

We can write

$$\begin{aligned} \tau_{23} &= -2\sqrt{2} \sin^2(\phi/2) J_x^{23} + i\sqrt{2} \sin\phi J_y^{23} \\ \tau_+ &= -2\sqrt{2} \sin^2(\phi/2) J_x^{12} - i\sqrt{2} \sin\phi J_y^{12} \end{aligned} \tag{C.0.34}$$

Where we define:

$$\begin{aligned} J_x^{ij} &= \frac{a_i^\dagger a_j + a_j^\dagger a_i}{2}, \\ J_y^{ij} &= \frac{a_i^\dagger a_j - a_j^\dagger a_i}{2}, \\ J_z^{ij} &= \frac{N_i - N_j}{2}, \end{aligned} \tag{C.0.35}$$

Which satisfies the algebra

$$\left[J_x^{ij}, J_y^{ij}\right] = -J_z^{ij}, \quad \left[J_z^{ij}, J_x^{ij}\right] = J_y^{ij}, \quad \left[J_z^{ij}, J_y^{ij}\right] = J_x^{ij} \tag{C.0.36}$$

Now,

$$\mathcal{J}_x^{ij}(t) = e^{-itH_{\text{eff}}} J_x^{ij} e^{itH_{\text{eff}}}, \quad \mathcal{J}_y^{ij}(t) = e^{-itH_{\text{eff}}} J_y^{ij} e^{itH_{\text{eff}}} \tag{C.0.37}$$

To calculate

$$\mathcal{J}_x^{23}(t) = e^{-itH_{\text{eff}}} J_x^{23} e^{itH_{\text{eff}}} \tag{C.0.38}$$

We use $N_a - N_b = 2J_x^{23}$ to obtain

$$e^{-itH_{\text{eff}}} (N_a - N_b) e^{itH_{\text{eff}}} = N_a - N_b + (-it) [H_{\text{eff}}, N_a - N_b] + \frac{(-it)^2}{2!} [H_{\text{eff}}, [H_{\text{eff}}, N_a - N_b]] + ... \tag{C.0.39}$$

And define the operator

$$T \equiv J_{\text{eff}}^{-1} H_{\text{eff}} = 2A_+ + N_a - N_b = 2A_+ + 2J_x^{23} \tag{C.0.40}$$

Such that

$$[T, N_a - N_b] = 2A_-, \quad [T, A_-] \ = 2(N_a - N_1) - A_+ \equiv \tilde{\Gamma}, \quad [T, \tilde{\Gamma}] = 9A_- \tag{C.0.41}$$

Using the above relations, we obtain

$$e^{-itH_{\text{eff}}} (N_a - N_b) e^{itH_{\text{eff}}} = N_a - N_b - \frac{2}{3} i \sin(3J_{\text{eff}} t) A_- - \frac{4}{9} \sin^2\left(\frac{3}{2} J_{\text{eff}} t\right) \tilde{\Gamma} \tag{C.0.42}$$

And hence

$$\mathcal{J}_x^{23}(t) = J_x^{23} - \frac{1}{3} i \sin(3J_{\text{eff}}\, t) A_- - \frac{2}{9} \sin^2\left(\frac{3}{2} J_{\text{eff}}\, t\right) \tilde{\Gamma}. \tag{C.0.43}$$

To calculate $\mathcal{J}_y^{23}(t)$ we define

$$B_\pm = \frac{a_1^\dagger b_{23} \pm b_{23}^\dagger a_1}{\sqrt{2}}, \quad \Gamma_1 \ = B_+ + 2J_z^{23}, \quad \Gamma_2 = B_- - 2J_y^{23} \tag{C.0.44}$$

Such that

$$\begin{aligned} &\left[A_+, J_y^{23}\right] = -\frac{B_+}{2}, \quad \left[J_x^{23}, B_+\right] = \frac{B_-}{2}, \quad \left[J_x^{23}, B_-\right] = \frac{B_+}{2}, \\ &[A_+, B_+] = -J_y^{23}, \quad [A_+, B_-] = J_z^{23}, \quad \left[A_+, J_z^{23}\right] = \frac{B_-}{2} \\ &\left[T, J_y^{23}\right] = -\Gamma_1, \quad [T, \Gamma_1] = 3\Gamma_2, \quad [T, \Gamma_2] = 3\Gamma_1 \end{aligned} \tag{C.0.45}$$

Using the above relations, we obtain

$$\mathcal{J}_y^{23}(t) = J_y^{23} + \frac{1}{3} i \sin\left(3J_{\text{eff}}\, t\right) \Gamma_1 + \frac{2}{3} \sin^2\left(\frac{3}{2} J_{\text{eff}} t\right) \Gamma_2 \tag{C.0.46}$$

For $t = \tau = \frac{\pi}{3J_{\text{eff}}}$, we have

$$\mathcal{J}_x^{23}(\tau) = J_x^{23} - \frac{2}{9}\tilde{\Gamma}, \quad \mathcal{J}_y^{23}(\tau) \;\; = J_y^{23} + \frac{2}{3}\Gamma_2 \tag{C.0.47}$$

We obtain $\mathcal{J}_x^{12}(\tau)$ and $\mathcal{J}_y^{12}(\tau)$ by cyclic permutation of the indexes in the above result.

Now, using the expectation values $\langle \mathcal{O} \rangle \equiv \langle N,0,0,0|\mathcal{O}|N,0,0,0\rangle$:

$$\begin{aligned} \left\langle \mathcal{J}_x^{23}(\tau) \right\rangle &= \frac{4}{9} N, \qquad \left\langle \mathcal{J}_y^{23}(\tau) \right\rangle = 0 \\ \left\langle \mathcal{J}_x^{12}(\tau) \right\rangle &= -\frac{2}{9} N, \qquad \left\langle \mathcal{J}_y^{12}(\tau) \right\rangle = 0 \end{aligned} \tag{C.0.48}$$

We obtain

$$\left\langle e^{-i\tau H_{\text{eff}}} \Lambda e^{i\tau H_{\text{eff}}} \right\rangle = -\frac{80}{81} \sin^2(\phi/2) \tag{C.0.49}$$

And finally, we obtain the expression for the interference fringe:

$$\frac{\langle N_1 \rangle}{N} = \frac{1}{N} \left\langle N,0,0,0 \left| e^{-i\tau H_{\text{eff}}} \tilde{N}_1(\tau) e^{i\tau H_{\text{eff}}} \right| N,0,0,0 \right\rangle = 1 - \frac{80}{81} \sin^2(\phi/2) \tag{C.0.50}$$

From (C.0.25) we have $N_1(2\tau) = N_1$, and from (C.0.32) we find

$$e^{-i\tau H_{\text{eff}}} \tilde{N}_1(\tau) e^{i\tau H_{\text{eff}}} = N_1 + e^{-i\tau H_{\text{eff}}} \Lambda e^{i\tau H_{\text{eff}}}, \tag{C.0.51}$$

The last term can be written as

$$\begin{aligned} & e^{-i\tau H_{\text{eff}}} \Lambda e^{i\tau H_{\text{eff}}} = -\alpha \mathcal{J}_x^{23}(\tau) + \beta \mathcal{J}_y^{23}(\tau) + \frac{\alpha}{2} \mathcal{J}_x^{12}(\tau) + \frac{\beta}{2} \mathcal{J}_y^{12}(\tau) \\ & \alpha = \frac{16}{9} \sin^2(\phi/2), \quad \beta = i\frac{8}{9} \sin\phi \end{aligned} \tag{C.0.52}$$

Explicitly, the above operators are

$$\begin{aligned} \mathcal{J}_x^{23}(\tau) &= J_x^{23} - \frac{2}{9} \left[2\left(a_{23}^\dagger a_{23} - N_1 \right) - \left(\frac{a_1^\dagger a_{23} + a_{23}^\dagger a_1}{\sqrt{2}} \right) \right] \\ \mathcal{J}_y^{23}(\tau) &= -\frac{1}{3} J_y^{23} + \frac{\sqrt{2}}{3} \left(a_1^\dagger b_{23} - b_{23}^\dagger a_1 \right) \\ \mathcal{J}_x^{12}(\tau) &= J_x^{12} - \frac{2}{9} \left[2\left(a_{12}^\dagger a_{12} - N_3 \right) - \left(\frac{a_3^\dagger a_{12} + a_{12}^\dagger a_3}{\sqrt{2}} \right) \right] \\ \mathcal{J}_y^{12}(\tau) &= -\frac{1}{3} J_y^{12} + \frac{\sqrt{2}}{3} \left(a_3^\dagger b_{12} - b_{12}^\dagger a_3 \right) \end{aligned} \tag{C.0.53}$$

Which implies

$$
\begin{aligned}
\mathcal{J}_x^{23}(\tau)|N,0,0,0\rangle =& \frac{4N}{9}|N,0,0,0\rangle + \frac{\sqrt{N}}{9}|N-1,1,0,0\rangle + \frac{\sqrt{N}}{9}|N-1,0,1,0\rangle \\
\mathcal{J}_y^{23}(\tau)|N,0,0,0\rangle =& -\frac{\sqrt{N}}{3}(|N-1,1,0,0\rangle - |N-1,0,1,0\rangle) \\
\mathcal{J}_x^{12}(\tau)|N,0,0,0\rangle =& -\frac{2N}{9}|N,0,0,0\rangle + \frac{5\sqrt{N}}{18}|N-1,1,0,0\rangle + \frac{\sqrt{N}}{9}|N-1,0,1,0\rangle \\
\mathcal{J}_y^{12}(\tau)|N,0,0,0\rangle =& \frac{\sqrt{N}}{6}|N-1,1,0,0\rangle + \frac{\sqrt{N}}{3}|N-1,0,1,0\rangle \\
\mathcal{J}_x^{23}(\tau)|N-1,1,0,0\rangle =& \frac{\sqrt{N}}{9}|N,0,0,0\rangle + (\cdots) \\
\mathcal{J}_y^{23}(\tau)|N-1,1,0,0\rangle =& \frac{\sqrt{N}}{3}|N,0,0,0\rangle + (\cdots) \\
\mathcal{J}_x^{12}(\tau)|N-1,1,0,0\rangle =& \frac{5\sqrt{N}}{18}|N,0,0,0\rangle + (\cdots) \\
\mathcal{J}_y^{12}(\tau)|N-1,1,0,0\rangle =& -\frac{\sqrt{N}}{6}|N,0,0,0\rangle + (\cdots) \\
\mathcal{J}_x^{23}(\tau)|N-1,0,1,0\rangle =& \frac{\sqrt{N}}{9}|N,0,0,0\rangle + (\cdots) \\
\mathcal{J}_y^{23}(\tau)|N-1,0,1,0\rangle =& -\frac{\sqrt{N}}{3}|N,0,0,0\rangle + (\cdots) \\
\mathcal{J}_x^{12}(\tau)|N-1,0,1,0\rangle =& \frac{\sqrt{N}}{9}|N,0,0,0\rangle + (\cdots) \\
\mathcal{J}_y^{12}(\tau)|N-1,0,1,0\rangle =& -\frac{\sqrt{N}}{3}|N,0,0,0\rangle + (\cdots)
\end{aligned}
\tag{C.0.54}
$$

Using the above results, we find

$$
\begin{aligned}
e^{-i\tau H_{\text{eff}}}\tilde{N}_1(\tau)e^{i\tau H_{\text{eff}}}|N,0,0,0\rangle =& N\,(1 - \frac{5\alpha}{9}|N,0,0,0\rangle + \frac{\sqrt{N}}{36}(\alpha - 9\beta)|N-1,1,0,0\rangle \\
& - \frac{\sqrt{N}}{18}(\alpha - 9\beta)|N-1,0,1,0\rangle, \\
e^{-i\tau H_{\text{eff}}}\tilde{N}_1(\tau)e^{i\tau H_{\text{eff}}}|N-1,1,0,0\rangle =& \sqrt{N}\frac{(\alpha + 9\beta)}{36}|N,0,0,0\rangle + (\cdots), \\
e^{-i\tau H_{\text{eff}}}\tilde{N}_1(\tau)e^{i\tau H_{\text{eff}}}|N-1,0,1,0\rangle =& -\sqrt{N}\frac{(\alpha + 9\beta)}{18}|N,0,0,0\rangle + (\cdots)
\end{aligned}
\tag{C.0.55}
$$

Thus, we obtain

$$
\begin{aligned}
\langle N_1^2\rangle &= \left\langle \left(e^{-i\tau H_{\text{eff}}f}\tilde{N}_1(\tau)e^{i\tau H_{\text{eff}}}\right)\left(e^{-i\tau H_{\text{eff}}}\tilde{N}_1(\tau)e^{i\tau H_{\text{eff}}}\right)\right\rangle \\
&= \left(1 - \frac{5\alpha}{9}\right)^2 N^2 + \frac{5}{36^2}\left(\alpha^2 - 81\beta^2\right)N, \\
\langle N_1\rangle^2 &= N^2\left(1 - \frac{5\alpha}{9}\right)^2
\end{aligned}
\tag{C.0.56}
$$

Which lead to

$$\begin{aligned}\Delta N_1 &= \sqrt{\langle N_1^2\rangle - \langle N_1\rangle^2} = N^{1/2}\frac{2\sqrt{5}}{81}\sqrt{80+\sec^2(\phi/2)}|\sin\phi| \\ \frac{d\langle N_1\rangle}{d\phi} &= -\frac{40}{81}N\sin\phi\end{aligned} \tag{C.0.57}$$

Substituting these results in the equation for the sensitivity we obtain:

$$\Delta\phi = \frac{\Delta N_1}{\left|\frac{d\langle N_1\rangle}{d\phi}\right|} = \frac{1}{N^{1/2}}\sqrt{1+\frac{1}{80}\sec^2(\phi/2)}. \tag{C.0.58}$$

Open-Arrangement Interferometer Setup

Consider a set of blue-detuned laser beams ($\lambda = 0.532$ μm) with potentials given by

$$V_{\text{latt}}(x,y,\lambda) = -V_1\sum_{j=1}^{3}\sin^2(kr\cdot u_j), \quad r=(x,y), \quad k=\frac{2\pi}{\lambda}, \tag{C.0.59}$$

Where u_j are a set of vectors

$$u_1=(0,1), \quad u_2=\left(\frac{\sqrt{3}}{2},\frac{1}{2}\right), \quad u_3=\left(\frac{\sqrt{3}}{2},-\frac{1}{2}\right) \tag{C.0.60}$$

And the distance between the nearest sites is $l=\frac{2\pi}{3k}=\frac{\lambda}{3}$.

We include a vertical counter-propagating red detuned laser beam with wavelength 2λ and large waist to control aspect ratio of potential.

Its potential is given by harmonic approximation

$$V_c(z) = -V_3 + V_3\frac{k^2z^2}{4} \tag{C.0.61}$$

To isolate four wells from the rest of the lattice and break integrability we use two gaussian laser beams with waist w (and depths $V_2-\epsilon$ and ϵ), with the potential is given by

$$V_{\hat{z}}(x,y,z,\lambda) = -\frac{V_2}{1+\frac{z^2}{R^2}}\exp\left[-\frac{2}{w^2}\frac{(x^2+y^2)}{1+\frac{z^2}{R^2}}\right], \quad R=\frac{\pi w^2}{\lambda}. \tag{C.0.62}$$

And the harmonic approximation is given by

$$V_{\hat{z}}(x,y,z,2\lambda) \approx -V_2 + \frac{2V_2}{w^2}\left(x^2+y^2\right) + \frac{V_2}{R^2}z^2, \quad R=\frac{\pi w^2}{2\lambda}=\frac{kw^2}{4} \tag{C.0.63}$$

Thus, one can generate an optical lattice with the topology of the $3+1$ integrable model (up to a constant $-V_2-V_3$):

$$\begin{aligned}V(x,y,z) =& V_{\text{latt}}(x,y+l,\lambda) + \left(\frac{k^2V_3}{4}+\frac{V_2}{R^2}\right)z^2 \\ &+ \frac{2(V_2-\epsilon)}{w^2}\left(x^2+y^2\right) + \frac{2\epsilon}{w^2}\left[x^2+(y-\Delta y)^2\right]\end{aligned} \tag{C.0.64}$$

Defining the parameter

$$\delta = 1 + \frac{2V_2\lambda^2}{3\pi^2 w^2 V_1} \tag{C.0.65}$$

the distance between the nearest sites is $d_{14} = \frac{l}{\delta} = \frac{2\pi}{3k\delta} = \frac{\lambda}{3\delta}$, and the distance between the next-nearest sites is $d_{12} = \sqrt{3}\frac{l}{\delta}$.

The harmonic approximation for the potential of well i, for $\epsilon = 0$ or $\Delta y = 0$, is given by

$$\begin{aligned} V^{(i)} &= \Lambda_i + \frac{m\omega_r^2}{2}\left[(x-x_i)^2 + (y-y_i)^2\right] + \frac{m\omega_z^2}{2}z^2, \quad i = 1,2,3,4 \\ \Lambda_i &= -\frac{9V_1}{4} + (1-\delta_{i,4})\frac{\pi^2\left(1-\delta^{-1}\right)V_1}{3} \end{aligned} \tag{C.0.66}$$

Where the trap frequencies are given by

$$\omega_r = \sqrt{\frac{3k^2}{2m}V_1\delta}, \quad \omega_z = \sqrt{\frac{2}{m}\left(\frac{k^2V_3}{4} + \frac{V_2}{R^2}\right)} \tag{C.0.67}$$

And the center of well i is given by

$$\begin{aligned} (x_1, y_1) &= \left(-\frac{\sqrt{3}l}{2\delta}, -\frac{l}{2\delta}\right), \quad (x_2, y_2) = \left(0, \frac{l}{\delta}\right) \\ (x_3, y_3) &= \left(\frac{\sqrt{3}l}{2\delta}, -\frac{l}{2\delta}\right), \quad (x_4, y_4) = (0,0) \end{aligned} \tag{C.0.68}$$

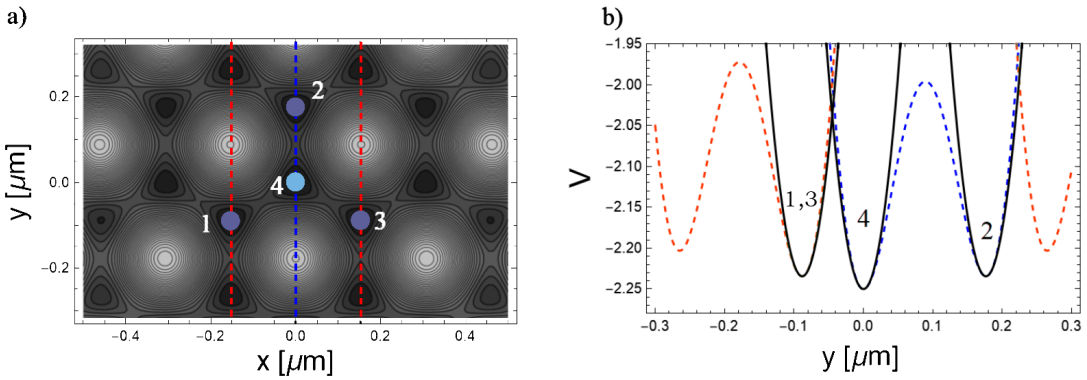

Figure 23: a) Contour plot of $V(x, y, 0)$ for $\lambda = 0.532\,\mu\text{m}, w = 2.0\,\mu\text{m}, V_1 = 1, V_2 = V_1, V_3 = V_1, \epsilon = V_1/2$ and $\Delta y = 0$. b) Plot of $V(0, x, 0)$ (blue dashed), $V(\pm x_2, x, 0)$ (red dashed) and harmonic approximation (black).

D Other Dynamics

In this appendix we present other dynamics using different parameters from the ones used in the interferometer models. The following subsections describe the behaviour of a closed-arrangement system with even N and two different open-arrangement cases with specific initial conditions that cause interesting dynamics.

Dynamics With Even N [Four-Well Closed Arrangement]

In this case the system takes twice as long to return to the initial distribution when compared to the example with odd N. We notice that the values of $\langle N_1 \rangle, \langle N_3 \rangle$ and $\langle N_2 \rangle, \langle N_4 \rangle$ at the peaks around $t = 6s$ are the opposite of image 6. This also reflects on the fidelity, which remains low at that point.

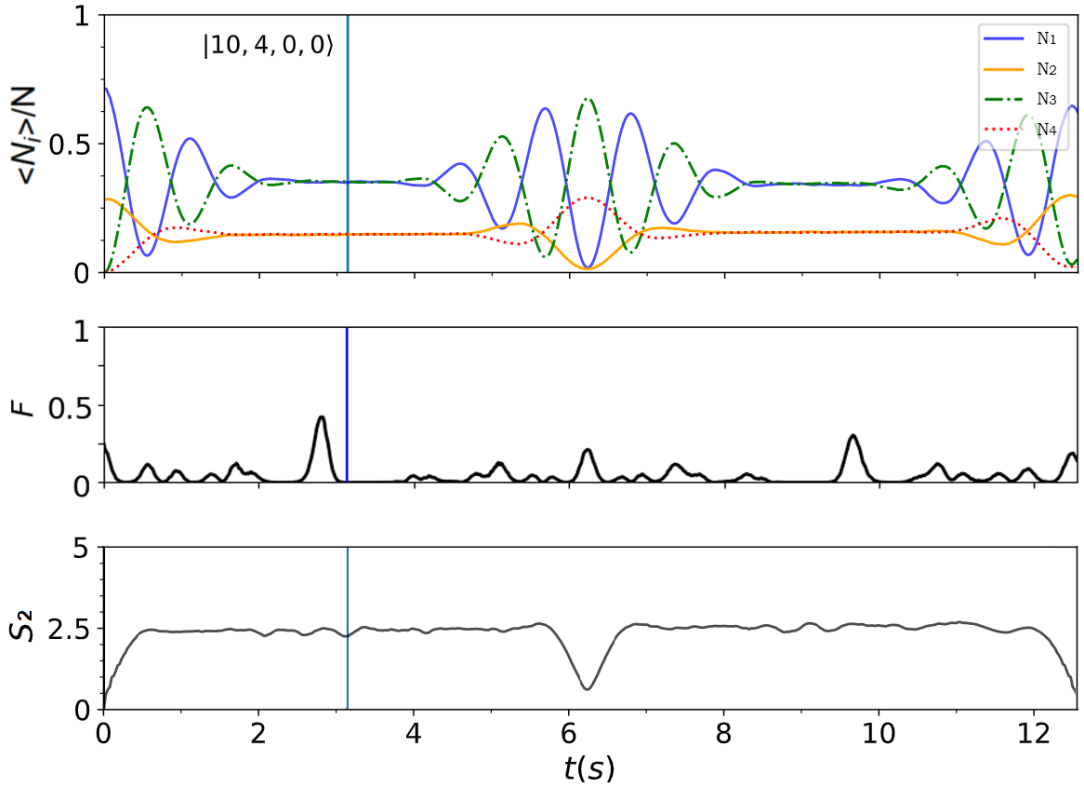

Figure 24: Dynamics for the initial state $|10, 4, 0, 0\rangle$, $U/\hbar = 76.519$ Hz and $J/\hbar = 73.219$ Hz. Vertical lines at $t = t_m$.

The graph for the fidelity is also missing the peak at t_m, present in the odd example (fig. 8), and the entanglement graph does not show a significant drop at that point.

The Case of M or P divisible by 3 [Four-Well Open Arrangement]

Starting with a combination of $1/3(|M,0,0,P\rangle+|0,M,0,P\rangle+|0,0,M,P\rangle)$ the state $|M/3,M/3,M/3,P\rangle$ or $|P/3,P/3,P/3,M\rangle$ will rise significantly above others depending on whether M or P is divisible by 3. (if both M and P are divisible by 3, the former will have preference). We can see this by plotting the fock state distribution histogram or heat-map with N_4 fixed to 1:

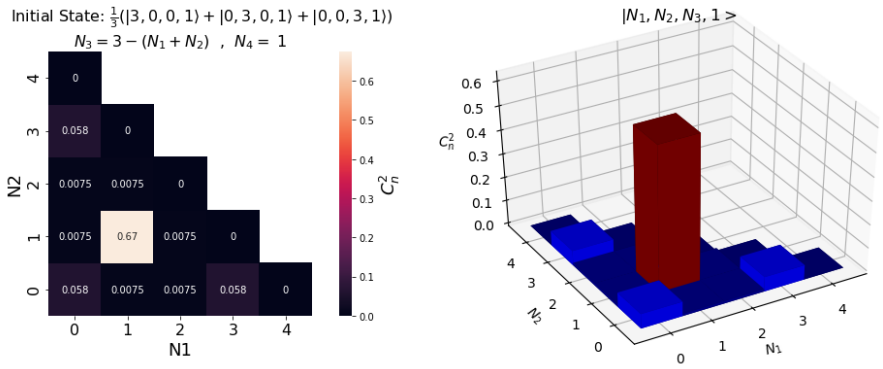

Figure 25: Histogram and heat-map for the initial state $(1/3)(|0031\rangle + |0301\rangle + |3001\rangle)$. The measurement is made at $t \approx 29s$, when the probability of state $|1111\rangle$ rises. $U/\hbar = 16$ Hz, $J/\hbar = 2$ Hz, The total number of bosons was kept small in order to obtain simpler graphs.

Although the fidelity is not ideal, this result indicates that the opposite dynamics ought to be valid, for example, starting with $|1111\rangle$ (where $M = 1+1+1 = 3$) will eventually lead to the appearance of $(1/3)(|0031\rangle + |0301\rangle + |3001\rangle)$. In cases with more bosons the configuration obtained is a combination of multiple trios, plus the original state.

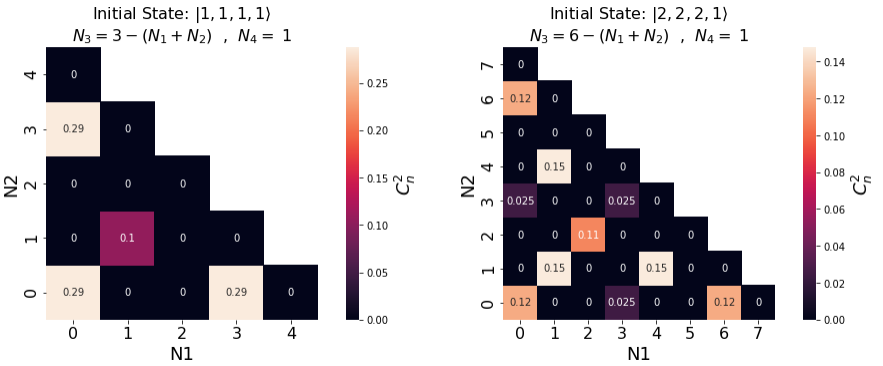

Figure 26: Heat-maps for $|1111\rangle$ and $|2221\rangle$. Dynamics simulation halted at $t \approx 93s$ and $t \approx 96s$ respectively. $U/\hbar = 16$ Hz, $J/\hbar = 2$ Hz.

The initial state never completely vanishes using this method, this can be changed by adding a new potential term to the hamiltonian, breaking its integrability:

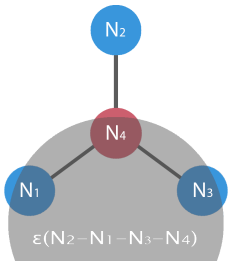

Figure 27: Diagram of the integrability break applied.

This yields Fock state combinations where the probability of the initial state is zero (or closer to it).

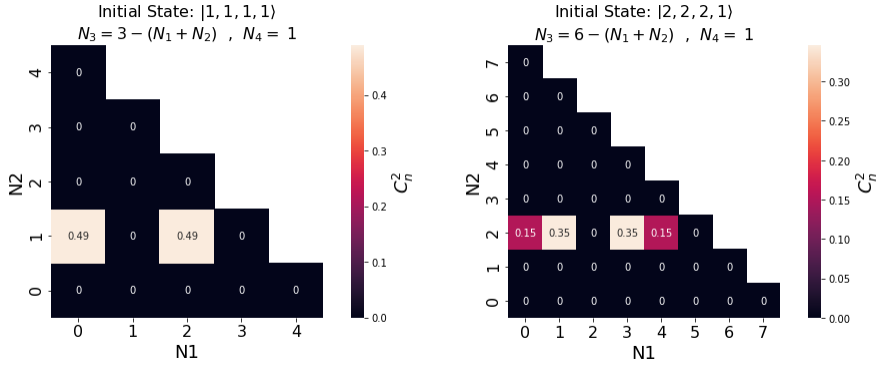

Figure 28: Heat-maps for $|1111\rangle$ and $|2221\rangle$ with the break of integrability. Dynamics simulation halted at $t \approx 89.5s$ and $t \approx 160s$ respectively. $|1111\rangle$ is the only state that yields a single pair. $U/\hbar = 16$ Hz, $J/\hbar = 2$ Hz, $\epsilon = 2$.

The two states obtained in the case with initial state $|1111\rangle$ and break of integrability are $|0121\rangle$ and $|2101\rangle$. These states have high probabilities, potentially allowing for physical applications.

The number of particles in each well for the case with initial state $|2, 2, 2, 1\rangle$ shown above remains constant. Another interesting state distribution occurs at $t \approx 112s$, where we obtain $|2, 2, 2, 1\rangle$, $|4, 2, 0, 1\rangle$, $|0, 2, 4, 1\rangle$.

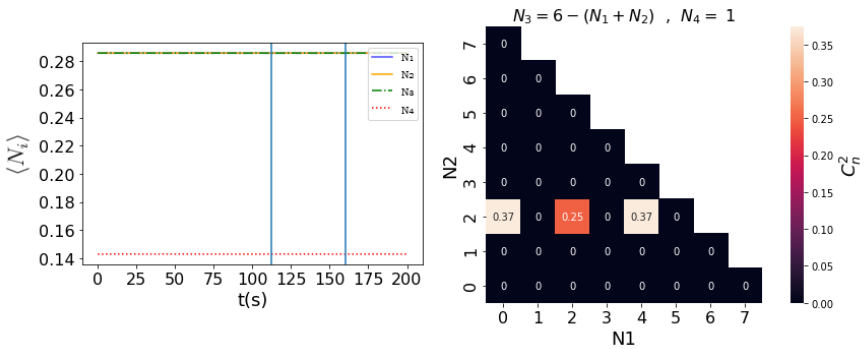

Figure 29: Left: Dynamics with the values for $\langle N_i \rangle$ constant, vertical lines at $t = 112s$ and $160s$. Right: The Fock state probabilities at $t = 112s$. $U/\hbar = 16$ Hz, $J/\hbar = 2$ Hz, $\epsilon = 2$.

The Case of $N_i = (N_i + N_j + N_k)/3$ [Four-Well Open Arrangement]

In this resonant regime, the number of bosons in wells 1,2 and 3 tend to oscillate around the mean $(N_1 + N_2 + N_3)/3$. By setting the initial number of bosons in N_i to $(N_i + N_j + N_k)/3$ we assure that this quantity will remain constant.

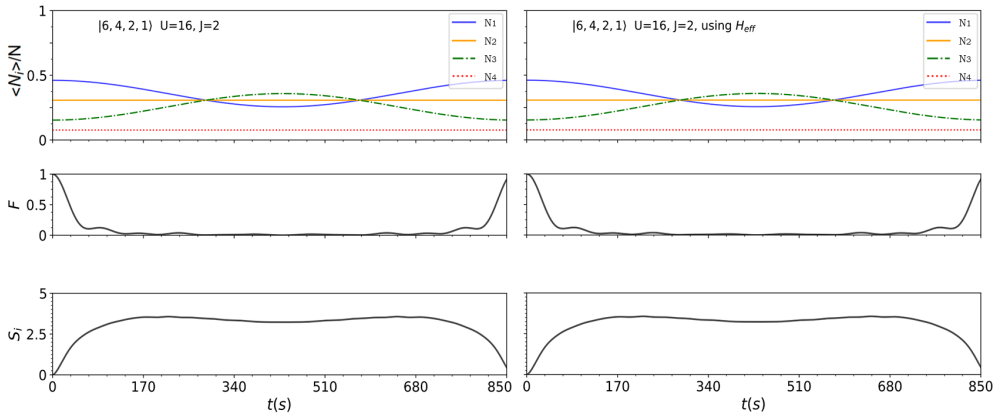

Figure 30: Simulations for dynamics of $\langle N_i \rangle$, fidelity and entanglement using H and H_{eff}. $U/\hbar = 16$ Hz, $J/\hbar = 2$ Hz.

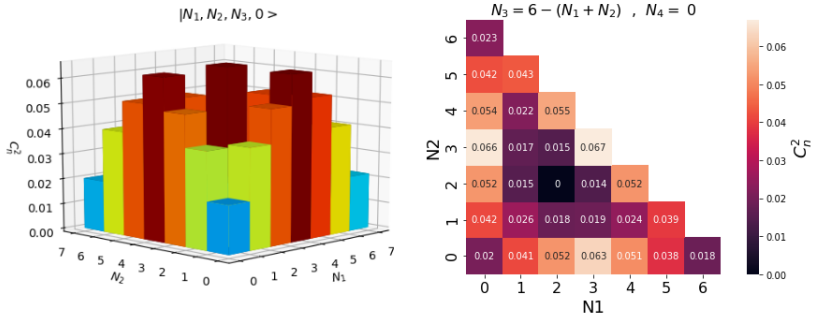

Figure 31: Fock state distribution when the lines for N_1, N_2, N_3 cross each other in the previous figure.

It is possible to change which well remains constant in Class A by introducing a break of integrability ($\epsilon(N_i - N_j - N_k - N_4)$) in the hamiltonian (see figure 27). This break can also be used to make the oscillations around the mean symmetric, alternating between two Fock states with probabilities ≈ 1:

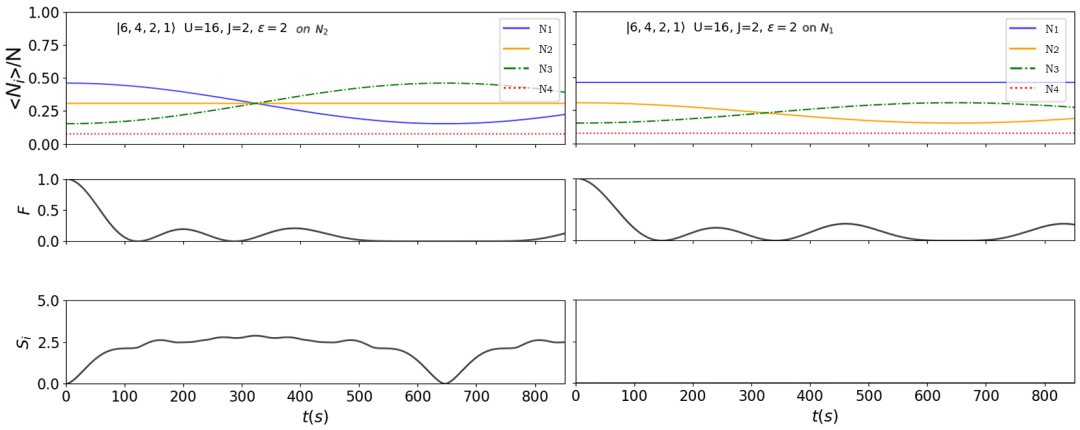

Figure 32: Left $[\epsilon(N_2 - N_1 - N_3 - N_4)]$: The states alternates between $|6, 4, 2, 1\rangle$ and $|2, 4, 6, 1\rangle$ with probability 1. Right $[\epsilon(N_1 - N_2 - N_3 - N_4)]$: It is possible to make N_1 (or N_3) constant instead. $U/\hbar = 16$ Hz, $J/\hbar = 2$ Hz, $\epsilon = 2$.

References

[1] S. N. Bose. Plancks gesetz und lichtquantenhypothese. Zeitschrift für Physik, 26(1):178–181, 1924.

[2] A Einstein. Sitzungsberichte der Preussischen Akademie der Wissenschaften, 1924.

[3] M. H. Anderson, J. R. Ensher, M. R. Matthews, C. E. Wieman, and E. A. Cornell. Observation of Bose-Einstein condensation in a dilute atomic vapor. Science, 269(5221):198–201, 1995.

[4] Durfee, D. S.; Ketterle, W. Experimental studies of Bose-Einstein condensation. Optics Express, Washington, v. 2, n. 8, p. 299-313. 1998.

[5] Bernd Wolf, Andreas Honecker, Walter Hofstetter, Ulrich Tutsch, and Michael Lang. Cooling through quantum criticality and many-body effects in condensed matter and cold gases. International Journal of Modern Physics B, 28(26):1430017, 2014.

[6] M. Batchelor, A. Foerster. Yang–Baxter integrable models in experiments: from condensed matter to ultracold atoms. Journal of Physics A: Mathematical and Theoretical 49 (17), 173001, 2016.

[7] A. Foerster, E. Ragoucy. Exactly solvable models in atomic and molecular physics. Nuclear Physics B 777 (3), 373, 2007.

[8] M. Duncan, A. Foerster, J. Links, E. Mattei, N. Oelkers, A. Tonel. Emergent quantum phases in a heteronuclear molecular Bose–Einstein condensate model. Nuclear Physics B 767 (3), 227, 2007.

[9] E. Schrödinger. Quantisierung als eigenwertproblem. Ann. Phys., 384(4):361–376, 1926.

[10] H. Bethe. Zur theorie der metalle. Zeitschrift für Physik, 71(3):205–226, 1931.

[11] C. N. Yang. Some exact results for the many-body problem in one dimension with repulsive delta-function interaction. Phys. Rev. Lett., 19:1312–1315, 1967.

[12] R. J. Baxter. Eight-vertex model in lattice statistics. Phys. Rev. Lett., 26:832–833, 1971.

[13] Elliott H. Lieb. Exact solution of the problem of the entropy of two-dimensional ice. Phys. Rev. Lett., 18:692–694, 1967.

[14] R. J. Baxter. Exactly solved models in statistical mechanics. In Integrable systems in statistical mechanics. World Scientific, 1985.

[15] L.D. Faddeev. Algebraic aspects of the bethe ansatz. International Journal of Modern Physics A, 10(13):1845– 1878, 1995.

[16] H. M. Babujian, A. Foerster, M. Karowski. Exact form factors of the SU(N) Gross–Neveu model and 1/N expansion, Nuclear Physics B 825 (3):396-425, 2010.

[17] Vladimir E Korepin and Fabian H L Essler. Exactly solvable models of strongly correlated electrons. World Scientific, 1994.

[18] J. Links, A. Foerster. Solution of a two-leg spin ladder system. Physical Review B 62 (1), 65, 2000.

[19] G. Santos, A. Foerster, I. Roditi, Z. V. T. Santos, and A. P. Tonel. Exactly solvable models for triatomic-molecular Bose-Einstein Condensates. Journal of Physics A: Mathematical and Theoretical 41 (29), 295003, 2008.

[20] D. Rubeni, A. Foerster, E. Mattei, I. Roditi. Quantum phase transitions in Bose–Einstein condensates from a Bethe ansatz perspective. Nuclear Physics B 856 (3) 698-715, 2012.

[21] L. Amico et. al. Roadmap on Atomtronics: State of the art and perspective. arXiv:2008.04439, 2021.

[22] Pepino, R.A. Advances in Atomtronics. Entropy 23, 534, 2021.

[23] L. D. Faddeev, E. K. Sklyanin, and L. A. Takhtajan. The quantum inverse problem method. 1. Theor. Math. Phys., 40:688–706, 1980. Teor. Mat. Fiz. 40, 194, 1979.

[24] A. Tonel, L. H. Ymai, A. Foerster, J. Links. Integrable model of bosons in a four-well ring with anisotropic tunneling. Journal of Physics A: Mathematical and Theoretical 48 (49), 494001, 2015.

[25] L. H. Ymai, A. P. Tonel, A. Foerster, and J. Links. Quantum integrable multi-well tunneling models. Journal of Physics A: Mathematical and Theoretical 50(26), 264001, 2017.

[26] D.S. Grun. Integrabilidade em Modelos de Tunelamento Quântico, Trabalho de Conclusão de Curso apresentado para Bacharel em Física, UFRGS, 2018.

[27] N.J. Lopes. Dinâmica em Modelos de Tunelamento Quântico, Trabalho de Conclusão de Curso apresentado para Bacharel em Física, UFRGS, 2020.

[28] J. Liouville. Note sur l'intégration des équations différentielles de la dynamique, présentée au bureau des longitudes le 29 juin 1853. Journal de Mathématiques Pures et Appliquées, 137–138, 1855.

[29] Michael Albiez, Rudolf Gati, Jonas Fölling, Stefan Hunsmann, Matteo Cristiani, and Markus K. Oberthaler. Direct observation of tunneling and nonlinear self-trapping in a single bosonic josephson junction. Phys. Rev. Lett., 95:010402, 2005.

[30] A. Tonel, J. Links and A. Foerster. Quantum dynamics of a model for two Josephson-coupled Bose-Einstein condensates. J. Phys. A 38 (6), 1235, 2005.

[31] A. Tonel, J. Links, and A. Foerster. Behaviour of the energy gap in a model of josephson coupled bose–einstein condensates. Journal of Physics A: Mathematical and General, 38(31):6879–6891, 2005.

[32] J. Links, A. Foerster, A.P. Tonel, G. Santos. The two-site Bose–Hubbard model. Annales Henri Poincaré 7 (7), 1591, 2006.

[33] G. Santos, A. Foerster, I. Roditi. A bosonic multi-state two-well model. Journal of Physics A: Mathematical and Theoretical 46 (26), 265206, 2013.

[34] D. Rubeni, J. Links, P.S. Isaac, A. Foerster. Two-site Bose-Hubbard model with nonlinear tunneling: Classical and quantum analysis. Physical Review A 95 (4), 043607, 2017.

[35] K. W. Wilsmann , L. H. Ymai, A. P. Tonel, J Links and A. Foerster. Control of tunneling in an atomtronic switching device. Commun. Phys. 1, 91, 2018. doi:10.1038/s42005-018-0089-1.

[36] A. P. Tonel, L. H. Ymai, K. W. Wilsmann, A. Foerster and J Links. Entangled states of dipolar bosons generated in a triple-well potential. SciPost Phys. Core 2 (003), 2020. doi:10.21468/SciPostPhysCore.2.1.003

[37] K. W. Wilsmann et. al. Quebra da integrabilidade para um modelo de tunelamento quântico de três poços, Dissertação de Mestrado em Física, UFRGS, 2017.

[38] Stickney, J. A., Anderson, D. Z. and Zozulya, A. A. Transistorlike behavior of a Bose-Einstein condensate in a triple-well potential. Phys. Rev. A 75, 013608, 2007.

[39] Hwang Lee , Pieter Kok and Jonathan P. Dowling. A quantum Rosetta stone for interferometry, Journal of Modern Optics, 49:14-15, 2325-2338, 2002.

[40] T. Lahaye, T. Pfau, L. Santos. Mesoscopic ensembles of polar bosons in triple-well potentials. arXiv:0911.5288v2, 2010.

[41] M. K. Olsen and A. S. Bradley. Quantum ultra-cold atomtronics. arXiv:1502.05097v1, 2015.

[42] M. K. Olsen and A. S. Bradley. Quantum ultracold atomtronics. PHYSICAL REVIEW A 91, 043635, 2015.

[43] Tobias Haug, Rainer Dumke, Leong-Chuan Kwek and Luigi Amico. Topological pumping in Aharonov–Bohm rings, Commun. Phys. 2, 127, 2019.

[44] D. S. Grun, K Wittmann W., L. H. Ymai, J. Links and A. Foerster. Atomtronic protocol designs for NOON states, arXiv:2102.02944, 2021.

[45] D. S. Grun, L. H. Ymai, K Wittmann W., A. P. Tonel, A. Foerster, and J. Links. Integrable atomtronic interferometry, arXiv:2004.11987, 2020.

[46] I. Brouzos and A.Foerster. Trace of broken integrability in stationary correlation properties, Physical Review A 89 (5) 053623, 2014.

[47] P. Jung and R.W. Helmes and A. Rosch. Transport in Almost Integrable Models: Perturbed Heisenberg Chains, Phys. Rev. Lett. 96 (6) 067202, 2006.

[48] B. Wilson, A. Foerster, C.C.N. Kuhn, I. Roditi and D. Rubeni. A geometric wave function for a few interacting bosons in a harmonic trap. Physics Letters A 378 (16-17): 1065-1070, 2014.